Universidad Autónoma de Madrid

Biblos-e Archivo
Repositorio Institucional UAM

Repositorio Institucional de la Universidad Autónoma de Madrid
https://repositorio.uam.es

Esta es la **versión de autor** del artículo publicado en:
This is an **author produced version** of a paper published in:

Food and Chemical Toxicology 138 (2020): 111202

DOI: https://doi.org/10.1016/j.fct.2020.111202

Copyright: © 2020 Elsevier Ltd.. This manuscript version is made available under the CC-BY-NC-ND 4.0 licence http://creativecommons.org/licenses/by-nc-nd/4.0/

El acceso a la versión del editor puede requerir la suscripción del recurso
Access to the published version may require subscription

Rumex dentatus L. phenolics ameliorate hyperglycemia by modulating hepatic key enzymes of carbohydrate metabolism, oxidative stress and PPARγ in diabetic rats

Rasha H. Elsayed[a#], Emadeldin M. Kamel[a#], Ayman M. Mahmoud [b#*], Ashraf A. El-Bassuony[a], May Bin-Jumah[c], Al Mokhtar Lamsabhi[d,e], Sayed A. Ahmed[a]

[a]Chemistry Department, Faculty of Science, Beni-Suef University, Beni-Suef 62514, Egypt.

[b]Physiology Division, Zoology Department, Faculty of Science, Beni-Suef University, Beni-Suef 62514, Egypt.

[c]Biology Department, College of Science, Princess Nourah bint Abdulrahman University, Riyadh 84428, Saudi Arabia.

[d]Departamento de Química, Módulo 13, Universidad Autónoma de Madrid, Campus de Excelencia UAM-CSIC Cantoblanco, Madrid 28049, Spain.

[e]Institute for Advanced Research in Chemical Sciences (IAdChem), Universidad Autónoma de Madrid, Madrid 28049, Spain.

#R.H.E., E.M.K. and A.M.M. participated as first author.

Corresponding author:

Ayman M. Mahmoud, PhD

Physiology Division, Zoology Department, Faculty of Science, Beni-Suef University, Salah Salim St., 62514, Beni-Suef, Egypt.

E-mail: ayman.mahmoud@science.bsu.edu.eg

Abstract

Rumex dentatus L. is a flowering plant with promising therapeutic effects. This study investigated the antioxidant efficacy of phenolic compounds isolated from *R. dentatus* L. *in vitro* and by conducting density function theory (DFT) studies to explore the mechanisms of action. The antioxidant, anti-inflammatory and antidiabetic effects of polyphenols-rich *R. dentatus* extract (RDE) were investigated in type 2 diabetic rats. Phytochemical investigation of the aerial parts of *R. dentatus* resulted in the isolation of one new and seven known compounds isolated for the first time from this species. All isolated phenolics showed *in vitro* radical scavenging activity. The antioxidant activity of the compounds could be oriented by the hydrogen atom transfer and sequential proton loss electron transfer mechanisms in gas and water phases, respectively. In diabetic rats, RDE attenuated hyperglycemia, insulin resistance and liver injury and improved carbohydrate metabolism. RDE suppressed oxidative stress and inflammation and upregulated PPARγ. *In silico* molecular docking analysis revealed the binding affinity of the isolated compounds toward PPARγ. In conclusion, the computational calculations were correlated with the *in vitro* antioxidant activity of *R. dentatus* derived phenolics. *R. dentatus* attenuated hyperglycemia, liver injury, inflammation and oxidative stress, improved carbohydrate metabolism and upregulated PPARγ in diabetic rats.

Keywords: Oxidative stress; Diabetes; Phenolics; Cytokines; PPARγ; DFT.

1. Introduction

Plants of the genus *Rumex* (sorrel, *Polygonaceae*) are distributed worldwide and have been used as vegetables. There are approximately 200 species belong to this genus and some possess beneficial pharmacologic properties (Vasas et al., 2015). *Rumex dentatus* L. is a flowering plant occurs in North Africa and Eurasia and commonly known as toothed dock (A Abou Elfotoh et al., 2013). *R. dentatus* is rich in bioactive constituents with well-acknowledged antioxidant effects (Elzaawely and Tawata, 2012; Humeera et al., 2013), and has been reported to suppress proliferation and induce apoptosis in breast cancer MDA-MB-231 cell line *in vitro* (Batool et al., 2017). In addition, Zhang *et al* have reported the anti-proliferation activity of an anthraquinone and naphthalene glucosides isolated from *R. dentatus* against breast cancer, melanoma, gastric cancer and oophoroma cell lines (Zhang et al., 2012). The alcoholic extracts of *R. dentatus* have shown potent antimicrobial activities against different pathogenic bacterial strains (Humeera et al., 2013), and ameliorated paracetamol-induced liver injury in mice (Saleem et al., 2014). Therefore, *R. dentatus* represents a promising source of bioactive compounds with beneficial therapeutic activities. Although *R. dentatus* showed a radical scavenging activity which was positively correlated with its phenolic content (Elzaawely and Tawata, 2012), little information is available on the isolation and characterization of phenolics from this plant. The leaves and roots of *R. dentatus* contain high levels of phenolic compounds as previously demonstrated by GC-MS and HPLC analyses (A Abou Elfotoh et al., 2013; Elzaawely and Tawata, 2012). The antioxidant activity of phenolics has been attributed to their radical-scavenging properties (Kamel et al., 2016). *In silico* investigation of the antioxidant potential of phenolic compounds can help disclosing the relation between the antioxidant activity and structure of phenolics (Kamel et al., 2016; Payán-Gómez et al., 2010). Besides the

commonly known routes for phenolics mechanisms of action as antioxidants, hydrogen atom transfer (HAT) and single-electron transfer followed by proton transfer (SET-PT), the sequential proton loss electron transfer (SPLET) has been proposed (Litwinienko and Ingold, 2005; Musialik and Litwinienko, 2005).

Diabetes mellitus (DM) is a metabolic disorder characterized by chronic hyperglycemia and impaired insulin action and/or release. Type 2 DM (T2DM) is the most prevalent form of DM and affects more than 380 million people worldwide (Cho et al., 2018). Chronic hyperglycemia in DM can lead to serious complications and increase the risk of developing liver diseases if not tightly controlled (Jellinger, 2007; Levinthal and Tavill, 1999). Besides hyperglycemia, impaired insulin action in peripheral tissues can increase the demand to insulin and lead to gradual destruction of β-cells (Halban et al., 2014). Hyperglycemia has also been associated with excessive generation of reactive oxygen species (ROS), oxidative stress and inflammation (Mahmoud et al., 2012). Excess ROS alter cell function, provoke lipid peroxidation (LPO), inflammation and cell death (Tiwari et al., 2013), reduce insulin release and impair insulin signaling, resulting in the development of serious diabetes complications (Newsholme et al., 2016). Therefore, counteracting hyperglycemia and its associated oxidative stress represents an effective strategy for the management of DM and its complications. In this context, the consumption of phenolic compounds and plant extracts rich in polyphenols ameliorated oxidative stress, inflammation and the metabolic derangements in DM (Ahmed et al., 2012; Ahmed et al., 2010; Mahmoud et al., 2017a; Mahmoud et al., 2012). Given its rich content of phenolics, *R. dentatus* can attenuate hyperglycemia and oxidative stress and improve insulin sensitivity in T2DM.

In this study, the antioxidant potential of phenolic compounds isolated from *R. dentatus* has been investigated and a density function theory (DFT) study on the structure-antioxidant activity relationship (SAR) was conducted to correlate the experimental findings with the theoretical predictions. In addition to the *in vitro* and *in silico* investigations, the antidiabetic potential of a phenolic-rich *R. dentatus* extract has been evaluated, pointing to its modulatory effect on peroxisome proliferator-activated receptor gamma (PPARγ), oxidative stress and inflammation. PPARγ is a ligand-inducible transcription factor that regulate the expression of multiple genes involved in metabolism and inflammation (Han et al., 2017). PPARγ activation increases insulin sensitivity, decreases blood glucose and lipids, and suppresses ROS generation and inflammation (Tontonoz and Spiegelman, 2008).

2. Materials and Methods

2.1. Phytochemical investigation

2.1.1. General

^{1}H-NMR and ^{13}C-NMR spectra of the investigated compounds were measured on Bruker AV-400 spectrometer operating at 400 MHz for ^{1}H-NMR and 100 MHz for ^{13}C-NMR. TMS was used as the internal standard. Chemical shift (δ) values were reported in (ppm) and coupling constants were calculated and expressed in Hz. HREI-MS mass data obtained by using Micromass Autospec (70 eV) spectrometer. UV data was recorded by Shimadzu UV–Vis 160i spectrophotometer. Optical rotation was measured by using (model: SR6) - USA polarimeter. FT-IR spectroscopic data were obtained from Nexus 670 FT-IR FT-Ramen spectrometer on KBr pellets.

2.1.2. Plant material

The aerial parts of *R. dentatus* L. were collected from Beni-Suef governorate between February and April 2017. The species was authenticated by the Botanists from the Botany Department and a voucher specimen was kept at the Herbarium of the Faculty of Science (Beni-Suef University, Egypt).

2.1.3. Extraction and isolation

The air-dried aerial parts of *R. dentatus* L. (1 kg) were powdered and extracted at room temperature with ethanol/water (7:3, 6 L x 4 times). The extracts were combined and evaporated *in vacuo* at 50 °C till dryness to give brownish sticky mass (350 g). The extract was dissolved in water and successively partitioned with dichloromethane (1 L x 4), ethyl acetate (EtOAc) (1 L x 4) and n-butanol (1 L x 4) to afford dichloromethane (9 g), EtOAc (8 g), n-butyl alcohol (39 g) and water-soluble extract (80 g), respectively. 7 g of the EtOAc extract was fractionated on silica gel column (100 x 3 cm, 200 g) using gradient elution started with EtOAc followed by EtOAc/methanol (MeOH) mixture of increasing polarity (9:1→ 0:10). 80 fractions were collected and then combined into 6 fractions (A→F) where the fractions were monitored by thin layer chromatography (TLC) and paper chromatography (PC). Fraction B (1.2 g) was subjected to silica gel column (60 x 3 cm, 70 g) and eluted with a gradient of n-hexane/EtOAc mixture to give 9 sub-fractions. Sub-fraction 6 (100 mg) was purified on silica column by n-hexane/EtOAc (6:4) to afford compound **2** (28 mg). Fraction D (1.5 g) was chromatographed on sephadex LH-20 column (60 x 3 cm) and eluted with MeOH-H_2O (2:8, 3:7, 4:6, 5:5, 6:4, 7:3, 8:2, 9:1 and 10:0) to yield 9 sub-fractions. Sub-fraction 3 (61 mg) was applied on sephadex LH-20 column using 30% MeOH to give compound **7** (15 mg). Sub-fraction 4 (165 mg) was

chromatographed on sephadex LH-20 column and eluted with saturated butanol to afford compound **3** (12 mg) and compound **6** (20 mg). Sub-fraction 5 (65 mg) was applied to sephadex LH-20 column and eluted with gradient of MeOH-H_2O (3:7, 4:6, 5:5, 6:4, 7:3) to afford compound **8** (5 mg). Fraction E (1.1 g) was subjected to sephadex LH-20 column (40 x 3.5 cm) and eluted with saturated butanol to give 4 sub-fractions. Sub-fraction 3 (43.5 mg) was purified on sephadex LH-20 column with 50% MeOH to afford compound **4** (11 mg) and sub-fraction 4 was also purified on sephadex LH-20 column with 25% MeOH to afford compound **5** (35 mg). Fraction F (40 mg) was purified over sephadex LH-20 column (50 x 1 cm) using 25% MeOH to give compound **1** (6 mg).

(S)- 4'-methylnonyl benzoate (1)

Yellow amorphous powder; $[\alpha]_D^{25}$ - 36.4 (*c* 0.09, MeOH); UV (MeOH) λ_{max} (log ε): 209.7 (4.98.16), 232 (5.11), 304.7 (4.87) and 368.8 (4.91) nm; IR ν_{max} cm^{-1} (KBr): 2984, 2817, 1741, 1631, 1561, 1473, 1085, 922 and 753 cm^{-1}; ^1H, ^{13}C NMR and selected HMBC data (Table 2); HR-ESI-MS (positive ion mode): *m/z* 262.2500 $[M+H]^+$ (calcd for $C_{17}H_{26}O_2$, 262.1933).

2.2. Computational methods

The quantum mechanical calculations were performed using the Gaussian 09 package and DFT was used for all calculations (Pv et al., 2017). The structure geometry of neutral compounds, cations, anions and radicals was optimized using B3LYP functional level and 6-311G + (d,p) was used as a basis set for these calculations. Frequency calculations were also performed at the same level to depict the stationary points, obtain zero-point energy (ZPE) and confirm that the ground states have no imaginary frequency. In addition, single point calculations were carried out on the optimized structures at 6-311G ++ (d,p) basis set in gas and water phase (ε = 1 and

78.4). Self-consistent reaction field (SCRF) calculations were employed for the solvation effect by using the polarizable continuum model (PCM) solvation method (Tomasi and Mennucci, 2002). The enthalpy of proton (H^+), hydrogen atom ($H^\bullet$) and electron (e^-) in gas phase and water phase were taken from the study of Rimarčík *et al* (Rimarčík et al., 2010).

2.3. Radical scavenging activity (RSA) assay

RSA of the isolated compounds against 2,2-diphenyl-1-picrylhydrazyl (DPPH) radicals was evaluated as previously reported (Brand-Williams et al., 1995) using rutin as a reference antioxidant.

2.4. *In vivo* antidiabetic effect of *R. dentatus* extract (RDE)

2.4.1. Experimental animals and induction of T2DM

Male Wistar rats, weighing 170-190 g, obtained from Vacsera (Giza, Egypt) were acclimatized for one week before the onset of the experiment. The rats were housed under standard conditions (23 ± 2°C and 50-60% humidity) and were supplied food and water *ad libitum*. The study protocol and procedures have been implemented in compliance with the National Institutes of Health guidelines (NIH publication No. 85–23, revised 2011) and were approved by the local Animal Care and Use Committee of Beni-Suef University. To induce T2DM, the rats were fed high fat diet (HFD; 58% fat, 25% protein and 17% carbohydrate) for 4 weeks followed by a single intraperitoneal (i.p.) injection of 35 mg/kg streptozotocin (STZ; Sigma, USA) dissolved in freshly prepared citrate buffer (pH 4.5). After 7 days, blood glucose was determined in overnight fasted rats 2 h following the oral administration of 3 g/kg glucose and rats having blood glucose levels ≥ 250 mg/dl were selected.

2.4.2. Experimental groups and treatments

To investigate the antidiabetic effect of RDE, the rats were divided into 7 groups (n=6) as following:

Group I (Control).

Group II (200 mg/kg RDE): received 200 mg/kg RDE orally for 4 weeks.

Group III (Diabetic).

Group IV (Diabetic + 50 mg/kg RDE): received 50 mg/kg RDE orally for 4 weeks.

Group V (Diabetic + 100 mg/kg RDE): received 100 mg/kg RDE orally for 4 weeks.

Group VI (Diabetic + 200 mg/kg RDE): received 200 mg/kg RDE orally for 4 weeks.

Group VII (Diabetic + PIO): received 10 mg/kg pioglitazone (PIO) (Abd El-Twab et al., 2016) orally for 4 weeks.

Groups I and II were fed normal chow diet and received a single injection of citrate buffer (pH 4.5). RDE and PIO were dissolved in 0.5% carboxymethyl cellulose (CMC). Groups I and III received 0.5% CMC orally for 4 weeks. The doses of RDE were selected based on previous studies employed *R. dentatus* methanolic extract at 250 and 500 mg/kg body weight to investigate its hepatoprotective effect in mice (Saleem et al., 2014). In another study, the *in vivo* antioxidant activity of the ethyl acetate fraction of another species, *R. tingitanus*, was studied in Wistar rats at a dose of 250 mg/kg body weight (Mhalla et al., 2018). Herein, we investigated the effect of 50, 100 and 200 mg/kg ethyl acetate fraction of *R. dentatus* in diabetic rats.

Twenty-four h after the last treatment, overnight fasted rats were sacrificed, and blood samples were collected on EDTA for glycated hemoglobin (HBA1c) estimation. Other blood samples were left to coagulate for serum separation. The rats were dissected, and the liver was removed to prepare 10% w/v homogenate in cold phosphate buffered saline (PBS). The homogenate was centrifuged, and the clear supernatant was collected for the determination of ROS, LPO, nitric oxide (NO), and the antioxidants reduced glutathione (GSH), superoxide dismutase (SOD) and catalase (CAT). Other samples were fixed in 10% neutral buffered formalin and others were kept frozen at -80°C for RNA isolation.

2.4.3. Oral glucose tolerance test (OGTT)

Blood samples were collected from the lateral tail vein of overnight fasted rats. The rats received 3 g/kg glucose solution and blood samples were collected after 30, 60, 90 and 120 min and glucose was measured according to the method of Trinder (Trinder, 1969) using commercially available kit (Spinreact, Spain).

2.4.4. Assay of HBA1c, insulin and HOMA-IR

Blood HbA1c% and serum insulin were determined using Biosystems (Spain) and RayBiotech (USA) assay kits, respectively. To evaluate the effect of RDE on insulin sensitivity, homeostasis model of insulin resistance (HOMA-IR) (Haffner, 2000) was calculated as following:

$$\mathrm{HOMA-IR} = \frac{\text{Fasting insulin } \left(\frac{\mu U}{ml}\right) \times \text{Fasting glucose } \left(\frac{mmol}{L}\right)}{22.5}$$

2.4.5. Assay of liver glycogen and glucose-metabolizing enzymes

Liver glycogen content was determined in the liver of control and diabetic rats according to the method of Seifter et al (Seifter et al., 1950). Hexokinase (Brandstrup et al., 1957), glucose-6-phosphatase (G-6-Pase) (Koide and Oda, 1959), fructose-1,6-biphosphatase (F-1,6-BPase) (Freedland and Harper, 1959) and glycogen phosphorylase (Stalmans and Hers, 1975) activities were assayed following previously described methods. Inorganic phosphorus (Pi) released during these assays was determined using Spinreact (Spain) reagent kit according to the method of Fiske and Subbarow (Fiske and Subbarow, 1925).

2.4.6. Assay of liver function and oxidative stress markers and cytokines

Serum alanine aminotransferase (ALT), aspartate aminotransferase (AST), alkaline phosphatase (ALP) and lactate dehydrogenase (LDH) were assayed using Spinreact (Spain) reagent kits. The levels of ROS were determined using 2′,7′-dichlorodihydrofluorescein diacetate (H_2DCF-DA) as previously described (Hozayen et al., 2019). Malondialdehyde (MDA), a marker of LPO, and NO were assayed in the liver homogenate following the methods of Preuss et al (Preuss et al., 1998) and Grisham et al (Grisham et al., 1996), respectively. Hepatic GSH content and activity of SOD and CAT were determined according to the methods of Beutler et al (Beutler et al., 1963), Marklund and Marklund (Marklund and Marklund, 1974) and Cohen et al (Cohen et al., 1970), respectively. TNF-α, IL-6 and IL-1β were determined using specific ELISA kits (R&D Systems, USA).

2.4.7. Histology

Immediately after dissection of the animals, samples from the liver were fixed in 10% neutral buffered formalin for 24 h. The fixed samples were processed for dehydration and embedding

in paraffin wax. 5-µm sections were cut using a rotary microtome, deparaffinized, rehydrated and stained with hematoxylin and eosin (H&E) for microscopic examination.

2.4.8. Gene expression

The effect of RDE on phosphoenolpyruvate carboxykinase (PEPCK), TNF-α, IL-6, IL-1β, iNOS, COX-2 and PPARγ in the liver of control and diabetic rats was determined by qRT-PCR (Mahmoud, 2014; Mahmoud et al., 2017b). Briefly, TRIzol reagent (Invitrogen, USA) was used to isolate RNA which was treated with RNase-free DNase (Qiagen, Germany) and then quantified on a nanodrop. RNA samples with A260/A280 nm > 1.7 were selected for cDNA synthesis that was amplified using SYBR Green master mix and the primers set listed in Table 1. The obtained data were analyzed by the $2^{-\Delta\Delta Ct}$ method (Livak and Schmittgen, 2001) and normalized to β-actin.

2.5. Molecular docking

Molecular docking analysis was conducted by Autodock Tools (ADT) v1.5.6 and AutoDock Vina software, and the obtained results were analyzed and visualized by using PyMOL v2.3.2. The 3D crystal structure of PPARγ was obtained from Protein Data Bank, (http://www.rcsb.org/pdb) (PDB, ID: 2PRG). The structure of the isolated compounds (**1**-**8**) was built using ChemDraw Ultra version 13.0 (ChemBioOffice modeling software, CambridgeSoft, UK) and then converted to .pdb 3D structure using UCSF Chimera (Pettersen et al., 2004). The protein receptor was prepared for docking by optimization which includes the addition of polar hydrogens and setting the grid box according to the best configuration of the active site amino acid residues (Nolte et al., 1998). The size of grid box was set at 38 x 38 x 46 (x,y,z). The center of the grid box was located at 52.893 x -34.142 x 12.877 (x,y,z).

2.6. Statistical analysis

All statistical comparisons were made by one-way ANOVA followed by Tukey's test and the differences were considered statistically significant at $P<0.05$. The results were presented as mean ± SEM (standard error of mean). The statistical analysis was carried out using GraphPad Prism 7 (La Jolla, CA, USA).

3. Results

3.1. Phytochemical study

Investigation of the EtOAc-soluble fraction revealed the isolation of one new compound (**1**) along with seven known compounds (**2**-**8**) (Fig. 1). The structure of the compounds was confirmed by ^{1}H-, ^{13}C- and 2D-NMR and spectroscopic tools (UV, MS and IR). The isolated compounds were identified as quercetin (**2**) (Renda et al., 2017), emodin-1-O-β-D-glucopyranoside (**3**) (El-Toumy et al., 2012), kaempferol-3-O-β-D-glucuronide (**4**) (Yang et al., 2010), querectin-3-O-β-D-glucuronide (**5**) (M. Soliman et al., 2002), querectin-3-O-β-D-glucopyranoside (**6**) (Islam et al., 2012), kaempferol (**7**) and resveratrol 3-glucoside (**8**) (Vastano et al., 2000).

Compound **1** is yellow amorphous, and its IR spectrum displayed strong peaks at 1741, 1631 and 1561, demonstrating the presence of an ester group. The molecular formula $C_{17}H_{26}O_2$ was obtained from the HR-ESI-MS data (*m/z* 262.2500, $[M+H]^+$, calcd 262.1933). ^{1}H and ^{13}C NMR and HMBC spectral analysis depicted in Table 2 indicated the presence of a monosubstituted benzene ring (δ_H 7.69, H-2 and H-6; 7.70-7.74, H-3, H-4 and H-5) confirmed by aromatic ^{13}C NMR signals at δ_c 129.13 (C-1), 127.08 (C-2, C-6), 125.96 (C-3, C-5) and 132.07 (C-4). The

presence of oxygenated methylene protons (H-1') was detected by a triplet PMR signal at δ_H 4.14 and a ^{13}C NMR at δ_c 67.88. The HR-ESI-MS peak at *m/z* = 105 diagnostic for the loss of alkoxy chain $C_{10}H_{21}O$. The characteristic pattern of methylnonyl benzoate group was deduced from the appearance of fifteen ^{13}C NMR signals that was detailed by DEPT experiment into two quaternary carbons, two methyl, seven methylene, three methine and one CH group. The ^{13}C NMR displayed most down field signal at δ_c 167.46 indicative for the presence of the carbonyl ester. The terminal methyl group was inferred by a ^1H NMR signal at δ_H = 0.88 (t, *J* = 6.2 Hz, C-10') and a ^{13}C NMR signal δ_C 11.36 (C-10'). Also, the methyl at C-4' was elucidated by signals at δ_H = 1.24 (m, C-5') and δ_C 14.26 (C-5'). Seven two-protons multiplets at δ_H 1.26-1.36 were attributed to methylene protons of the methylnonyl group and confirmed by the ^{13}C NMR signals in the range 22.55-31.75. From the HMBC correlation spectral analysis (Fig. 2), the location of methyl at position 4' of the nonyl group was estimated from the correlation of the methylene protons at δ_H 1.36 (H-2`) to $\delta_C$ 14.26 (C-5`). As well, H-1` ($\delta_H$ 4.14) showed strong correlation with $\delta_C$ 167.46 (CO) and $\delta_C$ 22.85 (C-3`) and weak correlation with δ_C 31.75 (C-2`). Furthermore, the terminal methyl resonance ($\delta_H$ =0.88, C-10`) displayed a strong HMBC correlation with C-8` (δ_C 23.7).The optical rotation of compound **1** ($[\alpha]_D^{25}$ - 36.4) was levorotatory that established the configuration of C-4' as 4'S. Alkaline hydrolysis of compound **1** afforded benzoic acid, mp 121-122 ºC (compared by Co TLC). Based on the described spectral data and conventional chemical reactions (alkaline hydrolysis), the structure of compound **1** was elucidated as **(***S***)**-4'-methylnonyl benzoate.

3.2. Computational studies and RSA

The isolated phenolics **2** and **4**-**7** contain the rings A, B and C of the flavone moiety (Fig. 1.). The OH groups in positions 5, 7 and 4′ are common in these compounds. Meanwhile,

compounds **2**, **5**, **6** and **7** show extra OH group at position 3′ for **2**, **5**, and **6** and position 3 for compound **7**. In addition, a fifth OH group appeared in the structure of compound **2**. Compounds **2** and **7** are flavonoids aglycones, while compounds **4**-**6** are flavonoids glycosides with a common position of the *O*-sugar moiety at position 3. Compound **3** is an anthraquinone glucoside with two hydroxyl substituents at positions 6 and 8, while compound **8** is a dihydroxystilbene glucoside with two OH groups at positions 5 and 4′. Whereas the primary elucidation of the optimized structures of the isolated phenolics was relied on the stereochemistry assessment provided through 1D and 2D NMR evaluation, many conformers for each compound were screened to find out the most stable conformer for each compound by altering the dihedral angle C2′–C1′–C2–C3 in compounds **2** and **4**-**7** and the angle C1′–C7–C8–C1 for compound **8**. With its structural features of stilbene, resveratrol (compound **8**) adopts (E) and (Z) isomeric conformers. Although the (E) isomer is the most biologically active and abundant form of resveratrol in nature, the optimized geometrical structures of (E) and (Z) isomers of this compound have been compared. Quantitative and qualitative analyses suggested that E-resveratrol exhibited stronger effects than Z-resveratrol in all experimental and computational assays. This fact is in agreement with the previously reported data (Lin et al., 2018).

The suggested mechanisms for the radical scavenging activity routes are represented in Figure 3. The Results of DFT calculations of BDE (kcal mol^{-1} at 298.15 K) of various hydroxyl groups in gas phase and aqueous medium of isolated compounds (**2**–**8**) are represented in Table 3. Homolytic cleavage of each OH of the phenolics (**2**-**8**) afforded five radicals in compound **2,** four radicals in compounds **5**-**7**, three radicals in compound **4** and two radicals in compounds **3** and **8**. Among all radicals**,** those obtained from the OH bond cleavage at position 4' are the most

stable for compounds **2**, **5**, **6** and **8**, while Flav-O radicals at positions 6, 7 and 3 are the most stable in compounds **3**, **4** and **7**, respectively. Phenoxy radicals at position 7 are the active site (lowest BDE) for compounds **4**-**6** in gas phase. This is might be associated with the linkage of sugar moiety to position 3 in these phenolics.

The calculated reaction enthalpies for the active sites in each compound (lowest BDE) of compounds under investigation in gas and water phases are represented in Table 4, respectively. Results assessment indicates that the homolytic dissociation of the OH is the most favorable mechanism in the gas phase. In contrast, the SPLET pathway is thermodynamically the most favorable mechanism in water phase because the first step energy demand of this mechanism is less than that required for homolytic OH bond cleavage. This indicates that phenolics in aqueous phase are guided to stimulate radical scavenging by the proton affinity of these entities. Interestingly, the highest antioxidant potential is compounds **2** which possess the lowest BDE active site. This is confirmed by the lowest IC_{50} value of this compound in the DPPH assay. In addition, compound **2** can afford five radical species because of the five hydroxyl substituents.

3.3. RDE attenuates hyperglycemia and improves insulin sensitivity in diabetic rats

OGTT and HbA1c% were determined to evaluate the anti-hyperglycemic potential of RDE in diabetic rats. Diabetic rats exhibited significant blood glucose elevation at all points of the OGTT (Fig. 4A) as revealed by the area under curve (AUC) analysis (Fig. 4B). Hyperglycemia was further confirmed by the significant elevation in HbA1c% (Fig. 4C). Treatment of the diabetic rats with RDE decreased blood glucose (Fig. 4A,B) and HbA1c% (Fig. 4C) significantly in a dose-dependent manner. In addition, PIO ameliorated hyperglycemia and HbA1c% in diabetic rats. Besides hyperglycemia, serum insulin was decreased (Fig. 4D) and

HOMA-IR value was increased significantly (Fig. 4E), effects that were reversed following treatment with 50, 100 and 200 mg/kg RDE or PIO.

3.4. RDE improves glucose metabolizing enzymes and increases glycogen in liver of diabetic rats

Hexokinase was significantly declined in HFD/STZ-induced rats when compared with the control rats ($P<0.001$; Fig. 5A). In contrast, the activities of G-6-Pase (Fig. 5B), F-1,6-BPase (Fig. 5C) and glycogen phosphorylase (Fig. 5E) and mRNA abundance of PEPCK (Fig. 5D) were increased in the liver of diabetic rats ($P<0.001$). Consequently, liver glycogen content was significantly ($P<0.001$) decreased in diabetic rats as depicted in Figure 5F. Treatment with RDE (50, 100 and 200 mg/kg) or PIO enhanced hexokinase and glycogen, and suppressed G-6-Pase, F-1,6-BPase, PEPCK and glycogen phosphorylase in liver of diabetic rats. Oral administration of 200 mg/kg RDE didn't affect the activity of the assayed enzymes or glycogen content in normal rats.

3.5. RDE prevents liver injury in diabetic rats

To evaluate the potential of RDE to prevent liver injury in diabetic rats, liver function markers were assayed, and a histopathological investigation was carried out. Serum transaminases, ALP and LDH were elevated in diabetic rats when compared with the control group ($P<0.001$; Fig. 6A-D). Treatment of diabetic rats with 50, 100 and 200 mg/kg RDE or PIO reduced serum ALT, AST, ALP and LDH.

Histopathological investigation supported the hepatoprotective efficacy of RDE. Examination of liver sections from diabetic rats revealed centrilobular hepatic vacuolation and fatty changes

(Fig. 7). Oral supplementation of 50 and 100 mg/kg RDE improved the histological architecture of the liver of diabetic rats which showed less vacuolations. The 200 mg/kg RDE as well as PIO remarkably prevented the histopathological alterations induced by diabetes in rat liver (Fig. 7).

3.6. RDE suppresses oxidative stress and enhances antioxidants in diabetic rats

ROS, MDA, NO and cellular antioxidants were determined to assess the protective effect of RDE against oxidative stress in diabetic rats (Fig. 8). Hepatic ROS, LPO and NO were increased in diabetic rats ($P<0.001$; Fig. 7A-C), whereas GSH content, and activities of SOD and CAT were markedly decreased (Fig. 8D-F). All doses of RDE as well as PIO were able to reduce hepatic ROS, LPO and NO, and enhance GSH, SOD and CAT. The effect of RDE on hepatic ROS, NO, SOD and CAT in diabetic rats was dose dependent. In normal rats, RDE didn't affect hepatic ROS, LPO, NO and cellular antioxidants (Fig. 8).

3.7. RDE attenuates inflammation in diabetic rats

Diabetic rats exhibited significantly elevated serum TNF-α (Fig. 9A), IL-1β (Fig. 9B) and IL-6 (Fig. 9C) when compared with the control rats ($P<0.001$). RDE and PIO decreased pro-inflammatory cytokines in serum of diabetic rats. RDE exerted a dose-dependent effect on serum TNF-α in diabetic rats.

The expression of pro-inflammatory cytokines, iNOS and COX-2 was assessed in the liver of control and treated rats. TNF-α, IL-1β, IL-6, iNOS and COX-2 mRNA abundance was significantly increased in the liver of HFD/STZ -induced rats ($P<0.001$; Fig. 9D-H). Oral supplementation of RDE or PIO downregulated the expression levels of all assayed inflammatory mediators. The effect of RDE on mRNA abundance of these mediators in the

liver of diabetic rats was dose dependent. Of note, oral supplementation of 200 mg/kg RDE didn't affect serum levels and mRNA abundance of the determined inflammatory mediators in normal rats.

3.8. RDE upregulates PPARγ expression in liver of diabetic rats

PPARγ gene expression was decreased in the liver of HFD/STZ diabetic rats when compared with the control group (Fig. 10A). All doses of RDE and PIO increased hepatic PPARγ mRNA abundance in diabetic rats.

Docking of *R. dentatus* isolated phytochemicals (**1**-**8**) onto PPARγ was carried out and the binding affinities and hydrogen bond interactions were analyzed (Table 5). The Isolated compounds showed binding affinities in the range of -7.2 kcal/mol to -8.7 kcal/mol with compound **8** formed the most stable complex with PPARγ. All compounds fitted the same pocket in PPARγ and showed binding toward the amino acids Phe226, Glu259, Arg288, Cys285, Ser289, Glu291, Ala292, Met329, Leu330, Glu295, Ile296, His323, Ile326, Tyr327, Leu333, SER342, Glu343, Thr268, Arg280, Phe363, Met364, His449 and Tyr473 (Fig. 10B). The compounds exhibited variable number of hydrogen bonding interactions (ranging from two to five) between their polar moieties and the amino acid residues (Table 5). The amino acids involved in the polar interactions of all isolated phytochemicals are Glu259, Arg288, Glu291, Thr 268, Ser342 and Glu343.

4. Discussion

This study investigated the antioxidant potential of compounds isolated from *R. dentatus* using *in vitro* and computational approaches. In addition, the anti-hyperglycemic, antioxidant and

anti-inflammatory effects of *R. dentatus* were evaluated in HFD/STZ-induced type 2 diabetic rats, pointing to the possible role of PPARγ.

Phytochemical analysis of *R. dentatus* resulted in the isolation of one new and seven known phenolic compounds. All isolated phenolic compounds exhibited a radical scavenging activity evidenced by the *in vitro* DPPH assay. The antioxidant properties of natural phenolics have been attributed to their potent radical scavenging activity which is associated with the existence of OH at specific position on the phenolic nucleus (Kamel et al., 2016). The flavonoid glycosides **4, 5** and **6** showed nearly similar active site BDE values but different IC_{50}. The main reason for this inconsistency is the different number of OH substituents. A second major reason is linked to the medium that can play a significant role in the antioxidant activity. For various OH groups in water, the BDE values order is nearly the same as that resulted for the gas phase.

At the active site on the phenolic compound core, homolytic or heterolytic OH bond cleavage may occur depending mainly on the reaction medium. The H-abstraction process is believed to be the main process underlying the antioxidant activity of these compounds (Barzegar, 2012). This study showed that the radicals obtained from the hydrogen abstraction at position 4' and 3' are commonly stable in the majority of phenolics and flavonoids (Kamel et al., 2016). This is attributed to the hydrogen bonding between one oxygen radical and one OH after H atom abstraction from one of the two OH substituents in positions C-3′ and C-4′ alternately. Furthermore, the existence of sugar causes planarity deviations and affects the stability of phenolics radicals (Alov et al., 2015). Consequently, aglycones could be more potent antioxidants than their corresponding glycosides. The main reason for this discrimination might be attributed to the electron withdrawing properties of the sugar moiety (Klein et al., 2009).

HAT, SET-PT and SPLET are the mechanisms suggested to understand the antioxidant activity of the phenolics (Nakanishi et al., 2005). The BDE values represent a tool for estimating the homolytic OH bond dissociation energy in HAT mechanism. The SPLET pathway includes heterolytic breakage of the OH bond followed by anion ionization (proton affinity (PA) + electron transfer enthalpy (ETE)), whereas SET-PT is an ionization of the phenolic compound followed by a proton transfer (ionization potential (IP) + proton dissociation enthalpy (PDE)). The overall energy demand of SET-PT or SPLET pathways is similar to HAT. Owing to the charge separation, SET-PT and SPLET are thermodynamically more favorable in polar media and are preferred destination for radicals with an elevated electron affinity (Amić et al., 2013; Zhang and Ji, 2006). Thus, the assessment of SAR of the isolated phenolics can be analyzed by evaluating the PA, ETE, IP, PDE and BDE. The findings of this study demonstrate that SPLET in aqueous medium and HAT in gas phase are the mechanisms behind the antioxidant activity of phenolics. Compounds **2** and **6-8** are the most potent antioxidant phenolics where the comparison between their PA and IP of the produced anion might prefer radical scavenging. On the other hand, the SET-PT pathway is the disfavored mechanism in all isolated phenolics. Moreover, the thermodynamic characteristics of these phenolics are affected by the nature of the H-abstraction site and the neighboring substituents.

Next, we investigated the potential of RDE to attenuate hyperglycemia, IR and oxidative stress, and to modulate carbohydrate metabolizing enzymes and PPARγ in type 2 diabetic rats. Hyperglycemia resulting from impaired insulin secretion and/or action is the characteristic feature of DM and can lead to serious complications if not tightly controlled (Jellinger, 2007). In this study, HFD/STZ-induced rats exhibited glucose intolerance and elevated blood HbA1c%, demonstrating hyperglycemia. In addition, these rats showed IR evidenced by the

significantly increased HOMA-IR. Elevated blood glucose and HbA1c%, and impaired insulin secretion and sensitivity have been previously demonstrated in HFD/STZ-induced rats (Guex et al., 2019; Mahmoud et al., 2012). This model has been acknowledged to mimic human T2DM (Lee et al., 2011) and is therefore widely accepted to evaluate the therapeutic effects of new agents. Interestingly, treatment of the diabetic rats with RDE improved glucose tolerance and decreased HbA1c%, indicating its effective anti-hyperglycemic effect. Assessment of HbA1c is a valuable test for the diagnosis and management of high blood glucose in diabetes and levels lower than 7% reveal good glycemic control (Association, 2014). In addition, RDE alleviated serum insulin levels and reduced HOMA-IR. Therefore, it is noteworthy assuming that increased insulin sensitivity following treatment with RDE attenuated hyperglycemia in diabetic rats.

Liver plays a central role in glucose homeostasis and the enzymes regulating hepatic glucose production represent potential targets for the control of blood glucose levels. In this context, uncontrolled hepatic glycogenolysis and gluconeogenesis and decreased peripheral glucose utilization resulting from impaired insulin secretion and/or action provoke hyperglycemia in diabetes (Nordlie et al., 1999). Thus, to explore the mechanism underlying the anti-hyperglycemic effect of RDE, we determined the activity of hepatic glucose-metabolizing enzymes and glycogen content in HFD/STZ-induced rats. The activity of hexokinase was significantly decreased, whereas G-6-Pase, F-1,6-BPase and glycogen phosphorylase were activated in diabetic rats. In accordance, previous studies have demonstrated a decrease in hepatic hexokinase activity and increased G-6-Pase and F-1,6-BPase in HFD/STZ-induced diabetic (Gothandam et al., 2019; Mishra et al., 2019). Decreased activity of hexokinase has been associated with impaired insulin secretion and IR, resulting in diminished glucose oxidation *via*

glycolysis and consequently hyperglycemia (Ahmed et al., 2010; Gupta et al., 1999). In contrast, G-6-Pase and F-1,6-BPase promote gluconeogenesis where F-1,6-BPase dephosphorylates fructose-1,6-bisphosphate into fructose-6-phosphate (Pilkis and Claus, 1991) and G-6-Pase catalyzes glucose-6-phosphate dephosphorylation to glucose (Roden and Bernroider, 2003). Consequently, glycogenolysis has also been provoked in the liver of HFD/STZ-induced rats as evidenced by the increased glycogen phosphorylase activity and decreased glycogen content. Exaggerated glycogenolysis and gluconeogenesis in diabetic rats indicate insulin deficiency and IR because insulin stimulates glycogen synthase and suppresses glycogen phosphorylase and G-6-Pase activities (Golden et al., 1979). Therefore, increased insulin release and sensitivity following treatment with RDE alleviated hexokinase, decreased F-1,6-BPase, G-6-Pase and glycogen phosphorylase, and restored hepatic glycogen content in diabetic rats. To investigate the anti-hyperglycemic effect of RDE separately from increased insulin sensitivity, PEPCK gene expression was investigated. PEPCK catalyzes the initial step in hepatic gluconeogenesis (Quinn and Yeagley, 2005) and its hepatic expression is upregulated in HFD/STZ-induced diabetes (Song et al., 2019). Accordingly, PEPCK mRNA abundance was increased in the liver of HFD/STZ diabetic rats in this study and this contributed to gluconeogenesis and hyperglycemia. Given that PEPCK is insulin-independent (Scott et al., 1998), its downregulation following treatment added support to the anti-hyperglycemic effect of RDE. Chronic hyperglycemia can lead to serious complications, including neuropathy, retinopathy and nephropathy and accelerate the progression of liver injury (Jellinger, 2007; Levinthal and Tavill, 1999). Accordingly, this study showed increased serum transaminases, ALP and LDH accompanied with histopathological alterations, particularly fatty changes, in the liver of diabetic rats. Hepatocyte injury in diabetes occurs as a result of excess lipid accumulation, hyperglycemia and hepatic IR

(Levinthal and Tavill, 1999). Liver function markers have been reported to increase in serum of HFD and/or STZ-induced rats (Sahin et al., 2019), and hepatic lipid infiltration occurs as a result of fatty acids accumulation, increased lipogenesis and impaired mitochondrial β-oxidation (Mohamed et al., 2016). Hyperglycemia can provoke liver injury by eliciting oxidative stress and inflammation (Mahmoud et al., 2012). Excess ROS can damage lipids, DNA and other cellular components, resulting in cell death (Tiwari et al., 2013). Additionally, ROS activate the redox-sensitive transcription factor NF-κB which elicits the expression of TNF-α, IL-1β, IL-6, iNOS, COX-2 and other inflammatory mediators. Therefore, hyperglycemia-mediated surplus ROS generation contributes significantly to liver injury in diabetes. The potential of ROS to induce hepatocyte dysfunction and damage is supported by studies showing attenuation of liver injury following ROS suppression (Aladaileh et al., 2019; Ranneh et al., 2019). Here, ROS, LPO and NO were increased, and the antioxidant defenses were diminished significantly in the liver of diabetic rats, demonstrating oxidative stress. Reduced cellular antioxidant defenses in the liver of diabetic rats has been previously demonstrated (Mahmoud et al., 2012; Sahin et al., 2019). In addition, TNF-α, IL-1β and IL-6, both serum levels and hepatic mRNA abundance, were increased in diabetic rats. Diabetic rats showed upregulation of hepatic COX-2 and iNOS gene expression which explained the increased NO levels. These findings demonstrate oxidative stress and inflammation in the liver of diabetic rats. In accordance, serum TNF-α and IL-6, and hepatic NF-κB expression were increased in diabetes induced by HFD and STZ in rats (Mahmoud et al., 2012; Sahin et al., 2019). Moreover, the circulating levels of TNF-α and IL-6 are known to increase in T2DM patients (Pickup et al., 2000). Increased pro-inflammatory cytokines has been associated with IR and impaired glucose tolerance. TNF-α suppresses insulin-stimulated peripheral glucose uptake, provokes hepatic glucose production (Lang et al., 1992), impairs

insulin action in muscles (Del Aguila et al., 1999) and increases lipolysis in adipocytes (Green et al., 1994). IL-6 impairs insulin signaling by reducing insulin receptor substrate (IRS)-1 tyrosine phosphorylation and protein kinase B/Akt phosphorylation in hepatocytes (Senn et al., 2002) and induces glucose intolerance (Müller et al., 2002). IL-1β has also been associated with the loss of β cell mass in T2DM (Dinarello et al., 2010) and directly induce IR in hepatocytes *in vitro* (Nov et al., 2010). Therefore, attenuation of oxidative stress and inflammation can ameliorate hyperglycemia and IR in T2DM. Treatment of the diabetic rats with different doses of RDE significantly reduced hepatic ROS, LPO and NO and boosted antioxidant defenses. In addition, RDE suppressed inflammation as evidenced by the decreased serum pro-inflammatory cytokines and hepatic mRNA abundance of TNF-α, IL-1β, IL-6, iNOS and COX-2. These findings demonstrate the potent antioxidant and anti-inflammatory efficacies of RDE. The improved insulin sensitivity and suppression of liver injury and lipid infiltration could be directly attributed to attenuation of oxidative stress and inflammation following RDE supplementation.

Previous studies have demonstrated the *in vitro* antioxidant activity of *R. dentatus* (Elzaawely and Tawata, 2012; Humeera et al., 2013). For instance, the EtOAc fractions of *R. dentatus* leaves and roots showed strong DPPH radical scavenging activity which was positively correlated with the high content of phenolic compounds (Elzaawely and Tawata, 2012). However, the studies investigated the antidiabetic and hepatoprotective efficacies of *R. dentatus* are scarce. In paracetamol-induced mice, *R. dentatus* methanolic extract at doses of 250 and 500 mg/kg reduced serum ALT, AST and ALP and prevented histological alterations (Saleem et al., 2014). Our findings present the first evidence that RDE ameliorated hyperglycemia, IR, oxidative stress, inflammation and liver injury, and modulated the activity of carbohydrate metabolizing enzymes in HFD/STZ-induced rats. These beneficial effects are

directly related to the active constituents of RDE, including emodin glucoside, quercetin, and kaempferol. Emodin and its glucosides have shown anti-inflammatory and antidiabetic effects (Lee et al., 2014; Xue et al., 2010). In HFD/STZ-induced mice, emodin improved glucose tolerance and insulin sensitivity (Xue et al., 2010) and emodin-6-O-β-D-glucoside suppressed high glucose-induced ROS generation and inflammation in endothelial cells *in vitro* (Lee et al., 2014). The anti-diabetic effect of quercetin has been well-demonstrated in different studies (reviewed in (Shi et al., 2019)). In HFD/STZ-induced rats (Gaballah et al., 2017) and type 2 diabetic *db*/*db* mice (Jeong et al., 2012), quercetin ameliorated hyperglycemia, IR and oxidative stress. Other putative antidiabetic mechanisms of quercetin include enhancement of glucose uptake, increase in insulin release and inhibition of α-glucosidase (reviewed in (Shi et al., 2019)). Moreover, kaempferol reduced blood glucose, increased insulin and attenuated oxidative stress in the liver of STZ-induced diabetic rats (Al-Numair et al., 2015). Recently, kaempferol has been reported to improve glucose tolerance and insulin sensitivity in HFD/STZ-induced diabetic mice and increase glucose uptake in adipocytes *in vitro* (Varshney et al., 2019).

To further explore the mechanisms underlying the antidiabetic effects of RDE, we investigated its effect on PPARγ gene expression in diabetic rats. In addition, we performed a molecular docking study to investigate the binding affinity of the isolated compounds with PPARγ. RDE increased hepatic PPARγ gene expression in diabetic rats. *In silico* analysis showed that all isolated compounds possess a binding affinity toward PPARγ. The amino acids involved in the polar interactions with all isolated phytochemicals are Glu259, Arg288, Glu291, Thr268, Ser342 and Glu343, most of which are crucial residues for ligand interactions and PPARγ activation (Álvarez-Almazán et al., 2017; Irudayaraj et al., 2016). Given that PPARγ agonists

such as PIO increases insulin sensitivity, ameliorate hyperglycemia and dyslipidemia in T2DM, prevent excessive lipid accumulation in peripheral tissues, and suppress pro-inflammatory cytokines (Tontonoz and Spiegelman, 2008), the antidiabetic effect of RDE is mediated, at least in part, *via* PPARγ activation. Besides these metabolic effects, activation of PPARγ can suppress inflammation, boost antioxidant enzymes and protect the liver (Hwang et al., 2005; Kersten et al., 2000; Okuno et al., 2010; Remels et al., 2009). PPARγ suppresses ROS production mediated *via* NADPH (Hwang et al., 2005), stimulates the gene expression of antioxidant enzymes (Okuno et al., 2010), diminish p65 nuclear translocation and NF-κB-dependent inflammatory genes transcription (Kersten et al., 2000; Remels et al., 2009).

5. Conclusions

Overall, 8 compounds including a new one, were detected in the EtOAc fraction of *R. dentatus*. The order of antioxidant activity of the isolated compounds estimated by computational analysis is dependent on the BDE values, nature and position of OH substituents. This arrangement is in a good agreement with the experimentally determined IC_{50} in the DPPH radical scavenging assay. The antioxidant mechanism of action of these phenolics is oriented by SPLET in the aqueous phase and by HAT in gas phase. However, the total energy demand of SPLET and SET-PT mechanisms is the same as that for the HAT pathway. Thus, we can rank the antioxidant efficacies of the isolated phenolics based on their BDE values. In addition, the current findings show for the first time that *R. dentatus* exhibited a potent antidiabetic activity in T2DM. Treatment of the diabetic rats with RDE ameliorated hyperglycemia, improved glucose tolerance and insulin sensitivity, increased liver glycogen and alleviated the activity of carbohydrate metabolizing enzymes. RDE suppressed excess ROS generation, oxidative stress and inflammation, prevented liver injury and enhanced antioxidant defenses in liver of diabetic

rats. Increased expression of hepatic PPARγ mediated, at least in part, the beneficial effects of RDE in diabetic rats. *In silico* study showed the binding affinity of *R. dentatus* phenolics toward PPARγ. Therefore, *R. dentatus* represent a promising lead for the management of T2DM, pending further investigations to explore the underlying mechanisms.

Supplementary Materials: Supplementary Figures 1-18: Spectral data of the isolated compounds, and Supplementary Figure 19: E and Z isomers of resveratrol.

Author Contributions: A.M.M. conceived the study, designed and performed animal experiments, carried out the biochemical, molecular and histologic studies, analyzed the data and prepared the figures. A.M.M. and E.M.K wrote the manuscript. R.H.E.; E.M.K. and A.A.E. carried out the phytochemical analysis. E.M.K. and A.L. performed the DFT studies. E.M.K. performed the molecular docking studies. M.B-J. provided resources, participated in the assays and acquired funding. A.M.M. and S.A.A. revised the manuscript. All authors read and approved the manuscript for publication.

Acknowledgments

The authors thank the Deanship of Scientific Research at Princess Nourah bint Abdulrahman University for supporting this research through the Fast-track Research Funding Program. This work has DGI Project no. CTQ2015-63997-C2, a generous allocation of computing time at the Centro de Computación Científica of the UAM is also acknowledged.

Conflicts of Interest

The authors declare no conflict of interest.

References

A Abou Elfotoh, M., Shams, K., Anthony, K., Shahat, A., T Ibrahim, M., M Abdelhady, N., Abdel-Azim, N., M Hammouda, F., El-Missiry, M., Saleh, M., 2013. Lipophilic Constituents of Rumex vesicarius L. and Rumex dentatus L.

Abd El-Twab, S.M., Mohamed, H.M., Mahmoud, A.M., 2016. Taurine and pioglitazone attenuate diabetes-induced testicular damage by abrogation of oxidative stress and up-regulation of the pituitary-gonadal axis. Canadian journal of physiology and pharmacology 94, 651-661.

Ahmed, O.M., Mahmoud, A.M., Abdel-Moneim, A., Ashour, M.B., 2012. Antidiabetic effects of hesperidin and naringin in type 2 diabetic rats. Diabetologia Croatica 41, 53-67.

Ahmed, O.M., Moneim, A.A., Mahmoud, A.M., Yazid, I.A., 2010. Antihyperglycemic, antihyperlipidemic and antioxidant effects and the probable mechanisms of action of Ruta graveolens infusion and rutin in nicotinamide-streptozotocin-induced diabetic rats. Diabetol. Croat. Diabetologia Croatica 39, 15-35.

Al-Numair, K.S., Chandramohan, G., Veeramani, C., Alsaif, M.A., 2015. Ameliorative effect of kaempferol, a flavonoid, on oxidative stress in streptozotocin-induced diabetic rats. Redox report : communications in free radical research 20, 198-209.

Aladaileh, S.H., Abukhalil, M.H., Saghir, S.A.M., Hanieh, H., Alfwuaires, M.A., Almaiman, A.A., Bin-Jumah, M., Mahmoud, A.M., 2019. Galangin Activates Nrf2 Signaling and Attenuates Oxidative Damage, Inflammation, and Apoptosis in a Rat Model of Cyclophosphamide-Induced Hepatotoxicity. Biomolecules 9, 346.

Alov, P., Tsakovska, I., Pajeva, I., 2015. Computational studies of free radical-scavenging properties of phenolic compounds. Current topics in medicinal chemistry 15, 85-104.

Álvarez-Almazán, S., Bello, M., Tamay-Cach, F., Martínez-Archundia, M., Alemán-González-Duhart, D., Correa-Basurto, J., Mendieta-Wejebe, J.E., 2017. Study of new interactions of glitazone's stereoisomers and the endogenous ligand 15d-PGJ2 on six different PPAR gamma proteins. Biochemical Pharmacology 142, 168-193.

Amić, D., Stepanić, V., Lučić, B., Marković, Z., Marković, J.M.D., 2013. PM6 study of free radical scavenging mechanisms of flavonoids: why does O–H bond dissociation enthalpy effectively represent free radical scavenging activity? Journal of molecular modeling 19, 2593-2603.

Association, A.D., 2014. Standards of medical care in diabetes--2014. Diabetes care 37 Suppl 1, S14-80.

Barzegar, A., 2012. Proton-coupled electron-transfer mechanism for the radical scavenging activity of cardiovascular drug dipyridamole. PloS one 7, e39660-e39660.

Batool, R., Aziz, E., Tan, B.K., Mahmood, T., 2017. Rumex dentatus Inhibits Cell Proliferation, Arrests Cell Cycle, and Induces Apoptosis in MDA-MB-231 Cells through Suppression of the NF-kappaB Pathway. Frontiers in pharmacology 8, 731.

Beutler, E., Duron, O., Kelly, B.M., 1963. Improved method for the determination of blood glutathione. The Journal of laboratory and clinical medicine 61, 882-888.

Brand-Williams, W., Cuvelier, M.-E., Berset, C., 1995. Use of a free radical method to evaluate antioxidant activity. LWT-Food science and Technology 28, 25-30.

Brandstrup, N., Kirk, J.E., Bruni, C., 1957. The hexokinase and phosphoglucoisomerase activities of aortic and pulmonary artery tissue in individuals of various ages. Journal of gerontology 12, 166-171.

Cho, N.H., Shaw, J.E., Karuranga, S., Huang, Y., da Rocha Fernandes, J.D., Ohlrogge, A.W., Malanda, B., 2018. IDF Diabetes Atlas: Global estimates of diabetes prevalence for 2017 and projections for 2045. Diabetes Research and Clinical Practice.
Cohen, G., Dembiec, D., Marcus, J., 1970. Measurement of catalase activity in tissue extracts. Analytical Biochemistry Analytical Biochemistry 34, 30-38.
Del Aguila, L.F., Claffey, K.P., Kirwan, J.P., 1999. TNF-α impairs insulin signaling and insulin stimulation of glucose uptake in C2C12 muscle cells. American Journal of Physiology - Endocrinology and Metabolism 276, E849-E855.
Dinarello, C.A., Donath, M.Y., Mandrup-Poulsen, T., 2010. Role of IL-1beta in type 2 diabetes. Current opinion in endocrinology, diabetes, and obesity 17, 314-321.
El-Toumy, S., S El Souda, S., K Mohamed, T., Brouard, I., Bermejo, J., 2012. Anthraquinone glycosides from Cassia roxburghii and evaluation of its free radical scavenging activity.
Elzaawely, A.A., Tawata, S., 2012. Antioxidant capacity and phenolic content of Rumex dentatus L. Grown in Egypt. Journal of Crop Science and Biotechnology 15, 59-64.
Fiske, C., Subbarow, Y., 1925. The colourimetric determination of phosphorus. Journal of Biological Chemistry 66, 375-400.
Freedland, R.A., Harper, A.E., 1959. Metabolic adaptations in higher animals. V. The study of metabolic pathways by means of metabolic adaptations. The Journal of biological chemistry 234, 1350-1354.
Gaballah, H.H., Zakaria, S.S., Mwafy, S.E., Tahoon, N.M., Ebeid, A.M., 2017. Mechanistic insights into the effects of quercetin and/or GLP-1 analogue liraglutide on high-fat diet/streptozotocin-induced type 2 diabetes in rats. Biomedicine and Pharmacotherapy 92, 331-339.
Golden, S., Wals, P.A., Okajima, F., Katz, J., 1979. Glycogen synthesis by hepatocytes from diabetic rats. The Biochemical journal 182, 727-734.
Gothandam, K., Ganesan, V.S., Ayyasamy, T., Ramalingam, S., 2019. Antioxidant potential of theaflavin ameliorates the activities of key enzymes of glucose metabolism in high fat diet and streptozotocin – induced diabetic rats. Redox Report 24, 41-50.
Green, A., Dobias, S.B., Walters, D.J.A., Brasier, A.R., 1994. Tumor necrosis factor increases the rate of lipolysis in primary cultures of adipocytes without altering levels of hormone-sensitive lipase. Endocrinology 134, 2581-2588.
Grisham, M.B., Johnson, G.G., Lancaster, J.R., Jr., 1996. Quantitation of nitrate and nitrite in extracellular fluids. Methods in enzymology 268, 237-246.
Guex, C.G., Reginato, F.Z., de Jesus, P.R., Brondani, J.C., Lopes, G.H.H., Bauermann, L.F., 2019. Antidiabetic effects of Olea europaea L. leaves in diabetic rats induced by high-fat diet and low-dose streptozotocin. J Ethnopharmacol 235, 1-7.
Gupta, D., Raju, J., Prakash, J., Baquer, N.Z., 1999. Change in the lipid profile, lipogenic and related enzymes in the livers of experimental diabetic rats: effect of insulin and vanadate. Diabetes Res Clin Pract 46, 1-7.
Haffner, S.M., 2000. Coronary heart disease in patients with diabetes. The New England journal of medicine 342, 1040-1042.
Halban, P.A., Polonsky, K.S., Bowden, D.W., Hawkins, M.A., Ling, C., Mather, K.J., Powers, A.C., Rhodes, C.J., Sussel, L., Weir, G.C., 2014. beta-cell failure in type 2 diabetes: postulated mechanisms and prospects for prevention and treatment. Diabetes care 37, 1751-1758.

Han, L., Shen, W.-J., Bittner, S., Kraemer, F.B., Azhar, S., 2017. PPARs: regulators of metabolism and as therapeutic targets in cardiovascular disease. Part II: PPAR-β/δ and PPAR-γ. Future Cardiol 13, 279-296.
Hozayen, W.G., Mahmoud, A.M., Desouky, E.M., El-Nahass, E.-S., Soliman, H.A., Farghali, A.A., 2019. Cardiac and pulmonary toxicity of mesoporous silica nanoparticles is associated with excessive ROS production and redox imbalance in Wistar rats. Biomedicine & Pharmacotherapy 109, 2527-2538.
Humeera, N., Kamili, A.N., Bandh, S.A., Amin, S.-u., Lone, B.A., Gousia, N., 2013. Antimicrobial and antioxidant activities of alcoholic extracts of Rumex dentatus L. Microbial Pathogenesis 57, 17-20.
Hwang, J., Kleinhenz, D.J., Lassegue, B., Griendling, K.K., Dikalov, S., Hart, C.M., 2005. Peroxisome proliferator-activated receptor-gamma ligands regulate endothelial membrane superoxide production. American journal of physiology. Cell physiology 288, C899-C905.
Irudayaraj, S.S., Stalin, A., Sunil, C., Duraipandiyan, V., Al-Dhabi, N.A., Ignacimuthu, S., 2016. Antioxidant, antilipidemic and antidiabetic effects of ficusin with their effects on GLUT4 translocation and PPARγ expression in type 2 diabetic rats. Chemico-biological interactions 256, 85-93.
Islam, M., Al-Amin, M., Mahboob, M., Siddiqi, A., Akter, S., Haque, M., Sultana, N., Chowdhury, A.M.S., 2012. Isolation of Quercetin-3-O-beta-d-glucopyranoside from the Leaves of Azadirachta Indica and Antimicrobial and Cytotoxic screening of the Crude Extracts.
Jellinger, P.S., 2007. Metabolic consequences of hyperglycemia and insulin resistance. Clinical Cornerstone 8, S30-S42.
Jeong, S.-M., Kang, M.-J., Choi, H.-N., Kim, J.-H., Kim, J.-I., 2012. Quercetin ameliorates hyperglycemia and dyslipidemia and improves antioxidant status in type 2 diabetic db/db mice. Nutr Res Pract 6, 201-207.
Kamel, E.M., Mahmoud, A.M., Ahmed, S.A., Lamsabhi, A.M., 2016. A phytochemical and computational study on flavonoids isolated from Trifolium resupinatum L. and their novel hepatoprotective activity. Food & function 7, 2094-2106.
Kersten, S., Desvergne, B., Wahli, W., 2000. Roles of PPARs in health and disease. Nature 405, 421-424.
Klein, E., Rimarcik, J., Lukes, V., 2009. DFT/B3LYP study of the O-H bond dissociation enthalpies and proton affinities of para- and meta-substituted phenols in water and benzene.
Koide, H., Oda, T., 1959. Pathological occurrence of glucose-6-phosphatase in serum in liver diseases. Clinica chimica acta; international journal of clinical chemistry 4, 554-561.
Lang, C.H., Dobrescu, C., Bagby, G.J., 1992. Tumor necrosis factor impairs insulin action on peripheral glucose disposal and hepatic glucose output. Endocrinology 130, 43-52.
Lee, W., Ku, S.-K., Lee, D., Lee, T., Bae, J.-S., 2014. Emodin-6-O-β-d--glucoside Inhibits High-Glucose-Induced Vascular Inflammation. Inflammation 37, 306-313.
Lee, Y.S., Li, P., Huh, J.Y., Hwang, I.J., Lu, M., Kim, J.I., Ham, M., Talukdar, S., Chen, A., Lu, W.J., Bandyopadhyay, G.K., Schwendener, R., Olefsky, J., Kim, J.B., 2011. Inflammation is necessary for long-term but not short-term high-fat diet-induced insulin resistance. Diabetes 60, 2474-2483.
Levinthal, G.N., Tavill, A.S., 1999. Liver Disease and Diabetes Mellitus. CLINICAL DIABETES 17, 73-81.
Lin, J., Li, X., Chen, B., Wei, G., Chen, D.J.M., 2018. E-Configuration Improves Antioxidant and Cytoprotective Capacities of Resveratrols. 23, 1790.

Litwinienko, G., Ingold, K., 2005. Abnormal solvent effects on hydrogen atom abstraction. 3. Novel kinetics in sequential proton loss electron transfer chemistry. The Journal of organic chemistry 70, 8982-8990.
Livak, K.J., Schmittgen, T.D., 2001. Analysis of relative gene expression data using real-time quantitative PCR and the 2(-Delta Delta C(T)) Method. Methods (San Diego, Calif.) 25, 402-408.
M. Soliman, F., H. Shehata, A., Khaleel, A., Ezzat, S., 2002. An Acylated Kaempferol Glycoside from Flowers of Foeniculum vulgare and F. Dulce.
Mahmoud, A.M., 2014. Hesperidin protects against cyclophosphamide-induced hepatotoxicity by upregulation of PPARγ and abrogation of oxidative stress and inflammation. Can J Physiol Pharmacol. 92, 717-724.
Mahmoud, A.M., Abd El-Twab, S.M., Abdel-Reheim, E.S., 2017a. Consumption of polyphenol-rich Morus alba leaves extract attenuates early diabetic retinopathy: the underlying mechanism. European journal of nutrition 56, 1671-1684.
Mahmoud, A.M., Ashour, M.B., Abdel-Moneim, A., Ahmed, O.M., 2012. Hesperidin and naringin attenuate hyperglycemia-mediated oxidative stress and proinflammatory cytokine production in high fat fed/streptozotocin-induced type 2 diabetic rats. Journal of Diabetes and its Complications 26, 483-490.
Mahmoud, A.M., Hussein, O.E., Hozayen, W.G., Abd El-Twab, S.M., 2017b. Methotrexate hepatotoxicity is associated with oxidative stress, and down-regulation of PPARgamma and Nrf2: Protective effect of 18beta-Glycyrrhetinic acid. Chemico-biological interactions 270, 59-72.
Marklund, S., Marklund, G., 1974. Involvement of the Superoxide Anion Radical in the Autoxidation of Pyrogallol and a Convenient Assay for Superoxide Dismutase. FEBS European Journal of Biochemistry 47, 469-474.
Mhalla, D., Zouari Bouassida, K., Chawech, R., Bouaziz, A., Makni, S., Jlaiel, L., Tounsi, S., Mezghani Jarraya, R., Trigui, M., 2018. Antioxidant, Hepatoprotective, and Antidepression Effects of Rumex tingitanus Extracts and Identification of a Novel Bioactive Compound. BioMed research international 2018, 7295848.
Mishra, C., Khalid, M.A., Fatima, N., Singh, B., Tripathi, D., Waseem, M., Mahdi, A.A., 2019. Effects of citral on oxidative stress and hepatic key enzymes of glucose metabolism in streptozotocin/high-fat-diet induced diabetic dyslipidemic rats. Iran J Basic Med Sci 22, 49-57.
Mohamed, J., Nazratun Nafizah, A.H., Zariyantey, A.H., Budin, S.B., 2016. Mechanisms of Diabetes-Induced Liver Damage: The role of oxidative stress and inflammation. Sultan Qaboos Univ Med J 16, e132-e141.
Müller, S., Martin, S., Koenig, W., Hanifi-Moghaddam, P., Rathmann, W., Haastert, B., Giani, G., Illig, T., Thorand, B., Kolb, H., 2002. Impaired glucose tolerance is associated with increased serum concentrations of interleukin 6 and co-regulated acute-phase proteins but not TNF-alpha or its receptors. Diabetologia 45, 805-812.
Musialik, M., Litwinienko, G., 2005. Scavenging of dpph• radicals by vitamin E is accelerated by its partial ionization: the role of sequential proton loss electron transfer. Organic Letters 7, 4951-4954.
Nakanishi, I., Kawashima, T., Ohkubo, K., Kanazawa, H., Inami, K., Mochizuki, M., Fukuhara, K., Okuda, H., Ozawa, T., Itoh, S., Fukuzumi, S., Ikota, N., 2005. Electron-transfer mechanism in radical-scavenging reactions by a vitamin E model in a protic medium.

Newsholme, P., Cruzat, V.F., Keane, K.N., Carlessi, R., de Bittencourt, P.I., Jr., 2016. Molecular mechanisms of ROS production and oxidative stress in diabetes. The Biochemical journal 473, 4527-4550.
Nolte, R.T., Wisely, G.B., Westin, S., Cobb, J.E., Lambert, M.H., Kurokawa, R., Rosenfeld, M.G., Willson, T.M., Glass, C.K., Milburn, M.V., 1998. Ligand binding and co-activator assembly of the peroxisome proliferator-activated receptor-γ. Nature 395, 137.
Nordlie, R.C., Foster, J.D., Lange, A.J., 1999. Regulation of glucose production by the liver. Annual review of nutrition 19, 379-406.
Nov, O., Kohl, A., Lewis, E.C., Bashan, N., Dvir, I., Ben-Shlomo, S., Fishman, S., Wueest, S., Konrad, D., Rudich, A., 2010. Interleukin-1beta may mediate insulin resistance in liver-derived cells in response to adipocyte inflammation. Endocrinology 151, 4247-4256.
Okuno, Y., Matsuda, M., Miyata, Y., Fukuhara, A., Komuro, R., Shimabukuro, M., Shimomura, I., 2010. Human catalase gene is regulated by peroxisome proliferator activated receptor-gamma through a response element distinct from that of mouse. Endocrine journal 57, 303-309.
Payán-Gómez, S.A., Flores-Holguín, N., Pérez-Hernández, A., Piñón-Miramontes, M., Glossman-Mitnik, D., 2010. Computational molecular characterization of the flavonoid rutin. Chemistry Central Journal 4, 12.
Pettersen, E.F., Goddard, T.D., Huang, C.C., Couch, G.S., Greenblatt, D.M., Meng, E.C., Ferrin, T.E., 2004. UCSF Chimera—a visualization system for exploratory research and analysis. Journal of computational chemistry 25, 1605-1612.
Pickup, J.C., Chusney, G.D., Thomas, S.M., Burt, D., 2000. Plasma interleukin-6, tumour necrosis factor α and blood cytokine production in type 2 diabetes. Life Sciences 67, 291-300.
Pilkis, S.J., Claus, T.H., 1991. Hepatic gluconeogenesis/glycolysis: regulation and structure/function relationships of substrate cycle enzymes. Annual review of nutrition 11, 465-515.
Preuss, H.G., Jarrell, S.T., Scheckenbach, R., Lieberman, S., Anderson, R.A., 1998. Comparative effects of chromium, vanadium and gymnema sylvestre on sugar-induced blood pressure elevations in SHR. Journal of the American College of Nutrition 17, 116-123.
Pv, R., Gunasekaran, S., Manikandan, A., 2017. Structural, Spectral analysis of Ambroxol using DFT methods.
Ranneh, Y., Akim, A.M., Hamid, H.A., Khazaai, H., Fadel, A., Mahmoud, A.M., 2019. Stingless bee honey protects against lipopolysaccharide induced-chronic subclinical systemic inflammation and oxidative stress by modulating Nrf2, NF-κB and p38 MAPK. Nutrition and Metabolism.
Remels, A.H., Langen, R.C., Gosker, H.R., Russell, A.P., Spaapen, F., Voncken, J.W., Schrauwen, P., Schols, A.M., 2009. PPARgamma inhibits NF-kappaB-dependent transcriptional activation in skeletal muscle. American journal of physiology. Endocrinology and metabolism 297, E174-E183.
Renda, G., Özgen, U., Ünal, Z., Sabuncuoglu, S., Palaska, E., Erdogan Orhan, I., 2017. Flavonoid derivatives from the aerial parts of Trifolium trichocephalum M. Bieb. and their antioxidant and cytotoxic activity.
Rimarčík, J., Lukeš, V., Klein, E., Ilcin, M., 2010. Study of the solvent effect on the enthalpies of homolytic and heterolytic N–H bond cleavage in p-phenylenediamine and tetracyano-p-phenylenediamine.
Roden, M., Bernroider, E., 2003. Hepatic glucose metabolism in humans--its role in health and disease. Best practice & research. Clinical endocrinology & metabolism 17, 365-383.

Sahin, N., Orhan, C., Erten, F., Tuzcu, M., Defo Deeh, P.B., Ozercan, I.H., Juturu, V., Kazim, S., 2019. Effects of allyl isothiocyanate on insulin resistance, oxidative stress status, and transcription factors in high-fat diet/streptozotocin-induced type 2 diabetes mellitus in rats. Journal of biochemical and molecular toxicology 33, e22328.
Saleem, M., Ahmed, B., Karim, M., Ahmed, S., Ahmad, M., Qadir, I., Syed, N., 2014. Hepatoprotective effect of aqeous methanolic extract of Rumex dentatus in paracetamol induced hepatotoxicity in mice. Bangladesh Journal of Pharmacology 9, 284-289.
Seifter, S., Dayton, S., et al., 1950. The estimation of glycogen with the anthrone reagent. Archives of biochemistry 25, 191-200.
Senn, J.J., Klover, P.J., Nowak, I.A., Mooney, R.A., 2002. Interleukin-6 induces cellular insulin resistance in hepatocytes. Diabetes 51, 3391-3399.
Shi, G.-J., Li, Y., Cao, Q.-H., Wu, H.-X., Tang, X.-Y., Gao, X.-H., Yu, J.-Q., Chen, Z., Yang, Y., 2019. In vitro and in vivo evidence that quercetin protects against diabetes and its complications: A systematic review of the literature. Biomedicine & Pharmacotherapy 109, 1085-1099.
Stalmans, W., Hers, H.G., 1975. The stimulation of liver phosphorylase b by AMP, fluoride and sulfate. A technical note on the specific determination of the a and b forms of liver glycogen phosphorylase. European journal of biochemistry 54, 341-350.
Tiwari, B.K., Pandey, K.B., Abidi, A.B., Rizvi, S.I., 2013. Markers of Oxidative Stress during Diabetes Mellitus. Journal of Biomarkers Journal of Biomarkers 2013, 1-8.
Tomasi, J., Mennucci, B., 2002. Self-consistent Reaction Field Methods.
Tontonoz, P., Spiegelman, B.M., 2008. Fat and beyond: the diverse biology of PPARgamma. Annu Rev Biochem. 2008;77:289-312. doi: 10.1146/annurev.biochem.77.061307.091829.
Trinder, P., 1969. Determination of Glucose in Blood Using Glucose Oxidase with an Alternative Oxygen Acceptor. Annals of Clinical Biochemistry: An international journal of biochemistry and laboratory medicine Annals of Clinical Biochemistry: An international journal of biochemistry and laboratory medicine 6, 24-27.
Varshney, R., Mishra, R., Das, N., Sircar, D., Roy, P., 2019. A comparative analysis of various flavonoids in the regulation of obesity and diabetes: An in vitro and in vivo study. Journal of Functional Foods 59, 194-205.
Vasas, A., Orbán-Gyapai, O., Hohmann, J., 2015. The Genus Rumex: Review of traditional uses, phytochemistry and pharmacology. Journal of ethnopharmacology 175, 198-228.
Vastano, B.C., Chen, Y., Zhu, N., Ho, C.-T., Zhou, Z., Rosen, R.T., 2000. Isolation and Identification of Stilbenes in Two Varieties of Polygonum cuspidatum. Journal of Agricultural and Food Chemistry 48, 253-256.
Xue, J., Ding, W., Liu, Y., 2010. Anti-diabetic effects of emodin involved in the activation of PPARgamma on high-fat diet-fed and low dose of streptozotocin-induced diabetic mice. Fitoterapia 81, 173-177.
Yang, J.-H., Kondratyuk, T.P., Marler, L.E., Qiu, X., Choi, Y., Cao, H., Yu, R., Sturdy, M., Pegan, S., Liu, Y., Wang, L.-Q., Mesecar, A.D., Van Breemen, R.B., Pezzuto, J.M., Fong, H.H.S., Chen, Y.-G., Zhang, H.-J., 2010. Isolation and evaluation of kaempferol glycosides from the fern Neocheiropteris palmatopedata. Phytochemistry 71, 641-647.
Zhang, H.-Y., Ji, H.-F., 2006. How vitamin E scavenges DPPH radicals in polar protic media. New journal of chemistry 30, 503-504.

Zhang, H., Guo, Z., Wu, N., Xu, W., Han, L., Li, N., Han, Y., 2012. Two Novel Naphthalene Glucosides and an Anthraquinone Isolated from Rumex dentatus and Their Antiproliferation Activities in Four Cell Lines.

Tables

Table 1. Primers used for qRT-PCR.

Gene	Forward Primer Sequence (5'-3')	Reverse Primer Sequence (5'-3')
TNF-α	AAATGGGCTCCCTCTCATCAGTTC	TCTGCTTGGTGGTTTGCTACGAC
IL-1β	GACTTCACCATGGAACCCGT	GGAGACTGCCCATTCTCGAC
IL-6	GACTTCCAGCCAGTTGCCTT	AAGTCTCCTCTCCGGACTTGT
iNOS	ATTCCCAGCCCAACAACACA	GCAGCTTGTCCAGGGATTCT
COX-2	TGATCTACCCTCCCCACGTC	ACACACTCTGTTGTGCTCCC
PEPCK	CGTTGGGAGCTAGGAGCAAA	CCCATCAGTGTCAGATGCGA
PPARγ	GGACGCTGAAGAAGAGACCTG	CCGGGTCCTGTCTGAGTATG
β-actin	AGGAGTACGATGAGTCCGGC	CGCAGCTCAGTAACAGTCCG

Table 2. ^{1}H, ^{13}C NMR and selected HMBC correlations of compound **1**[a].

Position	δ_H (*J* in H_Z)	δ_C	HMBC
1`	4.14 (t)	67.88	C-3`, CO, C-2`, C-4`
2`	1.36 (m)	31.75	C-4`, C-1`, C-5`
3`	1.32 (m)	22.85	
4`	1.62 (m)	38.54	
5`	1.24 (m)	14.26	C-3`, C-6`, C-2`, C-4`
6`	1.26 (m)	29.16	C-3`
7`	1.26 (m)	28.82	
8`	1.29 (m)	23.7	
9`	1.34 (m)	29.47	C-7`
10`	0.88 (t)	11.36	C-8`
1		129.13	
2, 6	7.69 (m, *J* = 4.02 H_Z)	127.08	
3, 5	7.70-7.74 (m, *J* = 4.02 H_Z)	125.96	
4	7.70-7.74 (m, *J* = 4.02 H_Z)	132.07	
(CO)		167.46	

[a] Measured in DMSO-d6 at 400 MHz (^{1}H-NMR) and 100 MHz (^{13}C-NMR).

Table 3. BDE values (in kcal mol^{-1} at 298.15 K) of different hydroxyl substituents of the isolated compounds (**2**-**8**) in gas and water phases.

	2		**3**		**4**		**5**		**6**		**7**		**8**	
	Gas	**water**	**Gas**	**water**	**Gas**	**water**	**Gas**	**water**	**Gas**	**water**	**Gas**	**water**	**Gas**	**water**
3-OH	**80.96**	**76.20**	—	—	—	—	—	—	—	—	82.49	76.93	—	—
5-OH	94.85	88.54			97.02	91.35	96.41	90.76	97.74	91.21	82.40	80.84	80.87	80.72
6-OH	—	—	87.58	87.1	—	—	—	—	—	—	—	—	—	—
7-OH	86.68	84.54	—	—	87.99	86.83	88.21	86.94	88.27	86.66	83.99	83.93	—	—
8-OH	—	—	102.66	100.4	—	—	—	—	—	—	—	—	—	—
3′-OH	83.88	79.85	—	—	—	—	95.92	87.88	95.63	87.97	—	—	—	—
4′-OH	72.56	73.12	—		95.73	90.53	96.70	86.68	95.04	86.63	79.73	78.47	76.39	74.92

Table 4. Reaction enthalpies (in kcal mol^{-1}) in gas and aqueous phases and RSA of the isolated compounds (**2**-**8**).

Compound	Active Site	BDE	SET-PT		SPLET		Active Site	BDE	SET-PT		SPLET		RSA IC_{50} (µg)
			IP	PDE	PA	ETE			IP	PDE	PA	ETE	
	Gas phase						Aqueous phase						
2	**4'-OH**	**72.56**	**167.14**	**221.34**	**318.03**	**70.45**	**4'-OH**	**73.13**	**77.92**	**5.06**	20.67	52.20	4.78
3	6-OH	87.58	179.97	223.54	317.22	86.28	6-OH	87.10	94.14	-7.30	17.86	68.98	96.18
4	7-OH	88.00	171.85	232.06	321.99	81.93	7-OH	86.83	86.68	-0.12	23.15	63.42	16.15
5	7-OH	88.21	170.75	233.38	320.59	83.54	4'-OH	86.68	84.59	1.83	19.56	66.85	11.27
6	7-OH	88.27	172.35	231.85	320.67	83.52	4'-OH	86.63	83.59	2.77	19.28	67.09	9.32
7	4'-OH	79.73	163.66	231.99	330.71	64.94	3-OH	76.93	76.54	0.13	32.26	44.41	8.54
8	4'-OH	76.39	158.43	233.88	327.04	65.27	4'-OH	74.92	72.94	1.72	28.48	46.17	10.28

Table 5. Binding affinities of phytochemicals isolated from *R. dentatus* (**1**-**8**) with PPARγ.

Compound	Affinity (kcal/mol)	Polar bonds
1	-7.2	2 (Arg288)
2	-8.1	3 (2 Glu291 and 1 Ser342)
3	-7.8	5 (2 Ser342, Glu343, Thr268 and Glu259)
4	-7.7	4 (2 Thr268, Ser342 and Glu291)
5	-8.0	5 (2 Glu291, 2Thr 268 and Ser342)
6	-7.7	5 (2 Glu291, 2 Thr268 and Ser342)
7	-8.2	3 (Glu291, Glu259 and Ser342)
8	-8.7	2 (Arg288 and Glu291)

Figure legends

Figure 1. Chemical structure of the compounds isolated from *R. dentatus*.

Figure 2. Representative HMBC correlations of compound **1**.

Figure 3. Suggested pathways for the radical scavenging mechanisms.

Figure 4. RDE attenuates hyperglycemia and improves insulin sensitivity in diabetic rats. RDE and PIO improved glucose tolerance (A,B), HbA1c% (C) and serum insulin (D), and decreased HOMA-IR (E) in diabetic rats. Data are Mean ± SEM, n = 6. $^{***}P<0.001$ versus Control and $^{\#}P<0.05$, $^{\#\#}P<0.01$ and $^{\#\#\#}P<0.001$ versus Diabetic.

Figure 5. RDE improves glucose metabolizing enzymes and increases glycogen in liver of diabetic rats. RDE and PIO enhanced hexokinase activity (A), suppressed G-6-Pase (B), F-1,6-BPase (C), PEPCK (D) and glycogen phosphorylase (E), and increased glycogen (F) in diabetic rats. Data are Mean ± SEM, n = 6. $^{***}P<0.001$ versus Control and $^{\#\#}P<0.01$ and $^{\#\#\#}P<0.001$ versus Diabetic.

Figure 6. RDE prevents liver injury in diabetic rats. RDE and PIO decreased serum ALT (A), AST (B), ALP (C) and LDH (D) in diabetic rats. Data are Mean ± SEM, n = 6. $^{***}P<0.001$ versus Control and $^{\#\#\#}P<0.001$ versus Diabetic.

Figure 7. RDE prevents histological alterations in liver of diabetic rats. Photomicrographs of H&E-stained liver sections in liver of Control (A) and RDE-treated rats (B) showing normal structure of hepatic lobule, hepatocytes and central vein, (C-D) diabetic rats showing centrilobular hepatic vacuolation of round border and fatty changes (arrows), and (E-H)

diabetic rats treated with 50 (E), 100 (F) and 200 mg/kg (G) RDE or PIO (H) showed remarkable improvement of liver structure with few hepatic vacuolations (arrows).

Figure 8. RDE suppresses oxidative stress and enhances antioxidants in diabetic rats. RDE and PIO decreased ROS (A), MDA (B) and NO (C), and increased GSH (D), SOD (E) and CAT (F) in liver of diabetic rats. Data are Mean ± SEM, $n = 6$. $^{***}P<0.001$ versus Control and $^{###}P<0.001$ versus Diabetic.

Figure 9. RDE attenuates inflammation in diabetic rats. RDE and PIO decreased serum TNF-α (A), IL-1β (B) and IL-6 (C), and the gene expression levels of TNF-α (D), IL-1β (E), IL-6 (F), iNOS (G) and COX-2 (H) in liver of diabetic rats. Data are Mean ± SEM, $n = 6$. $^{***}P<0.001$ versus Control and $^{###}P<0.001$ versus Diabetic.

Figure 10. RDE upregulates PPARγ expression in liver of diabetic rats. (A) RDE and PIO increased the gene expression levels of PPARγ in the liver of diabetic rats. Data are Mean ± SEM, $n = 6$. $^{***}P<0.001$ versus Control and $^{###}P<0.001$ versus Diabetic. (B) Molecular docking analysis showing the binding between compounds **1**-**8** and PPARγ.

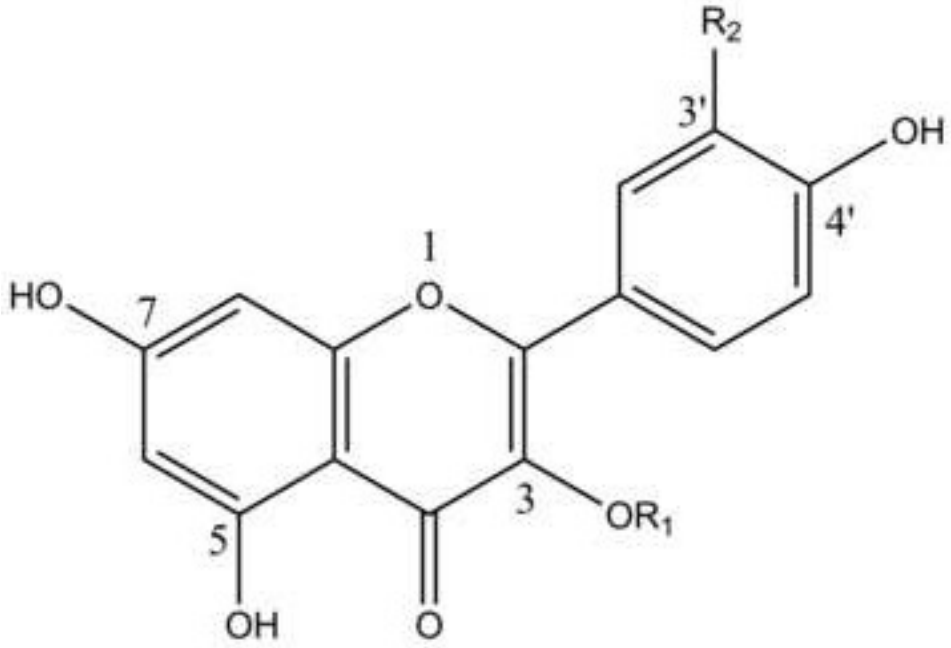

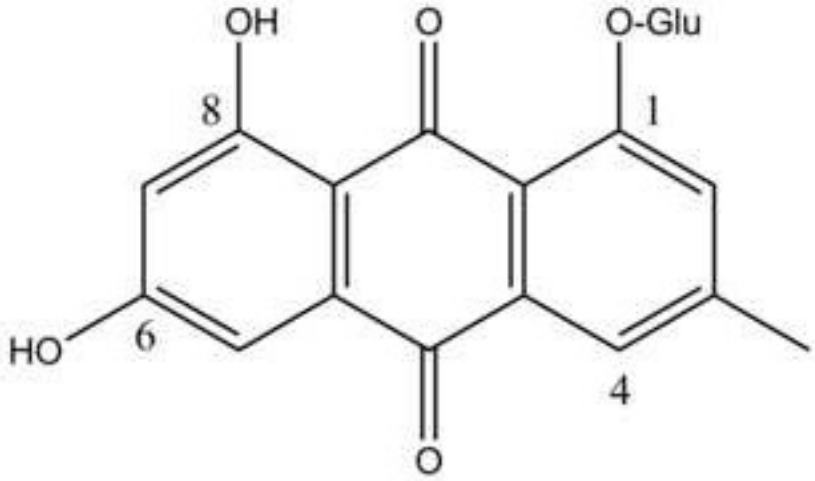

(3)

(2): R1= H R2= OH
(4): R1= glucuronic R2= H
(5): R1= glucuronic R2= OH
(6): R1= glucopyranoside R2= OH
(7): R1= H R2= H

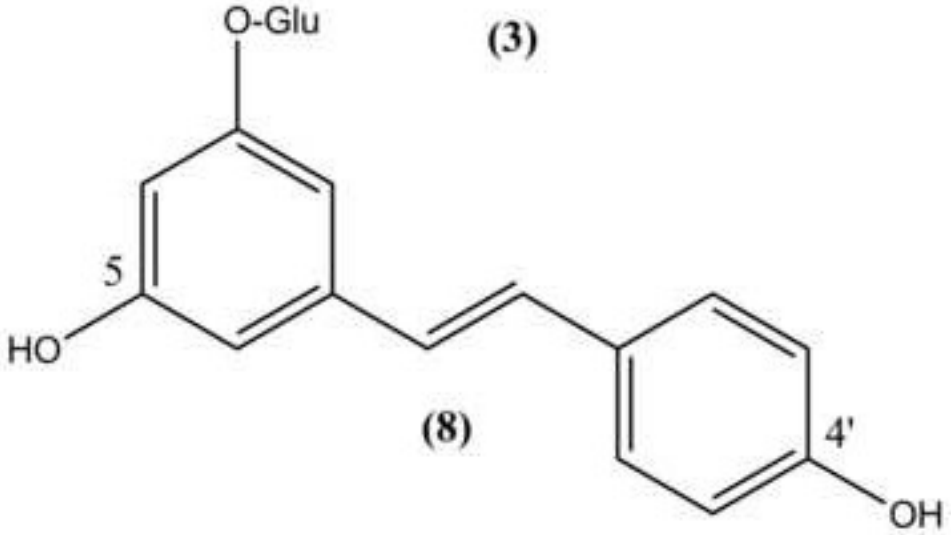

(8)

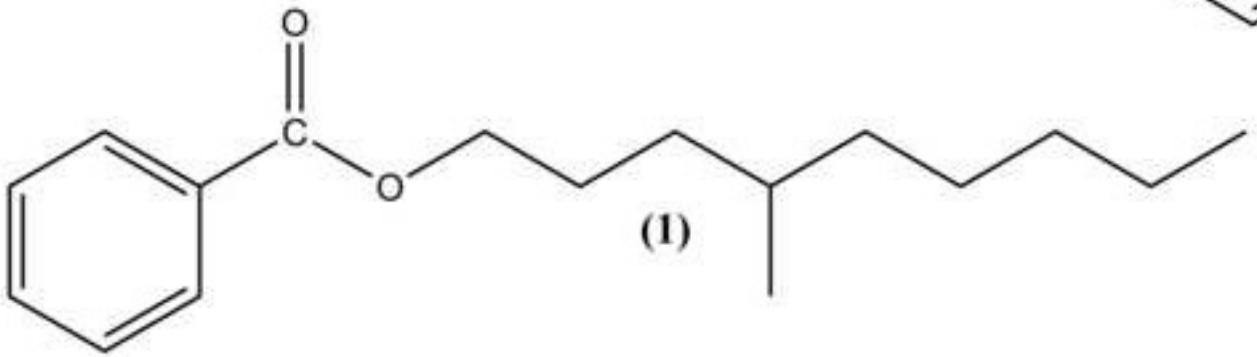

(1)

Figure 2

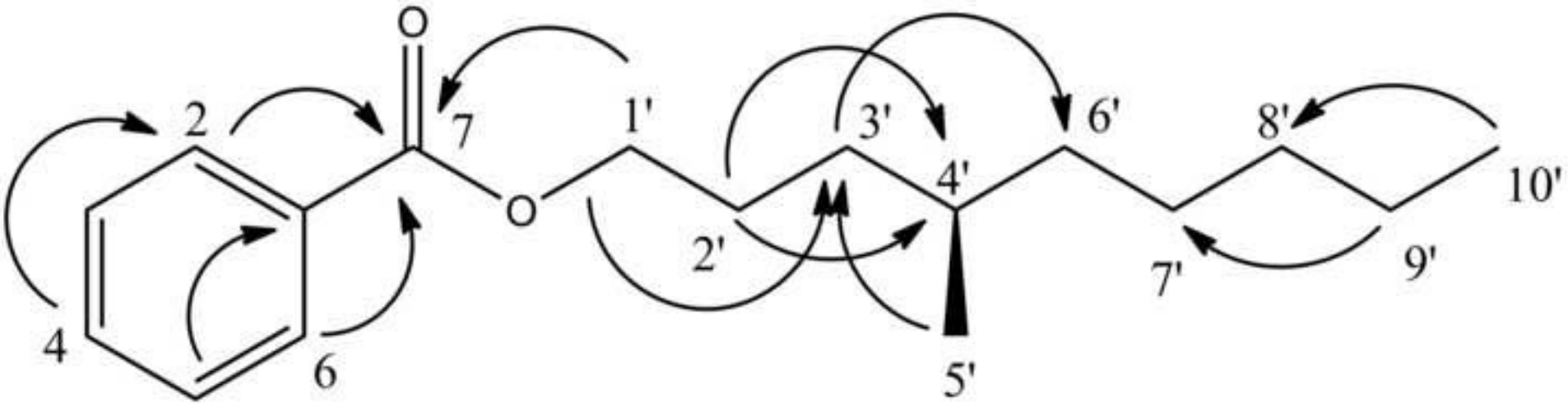

Figure 3

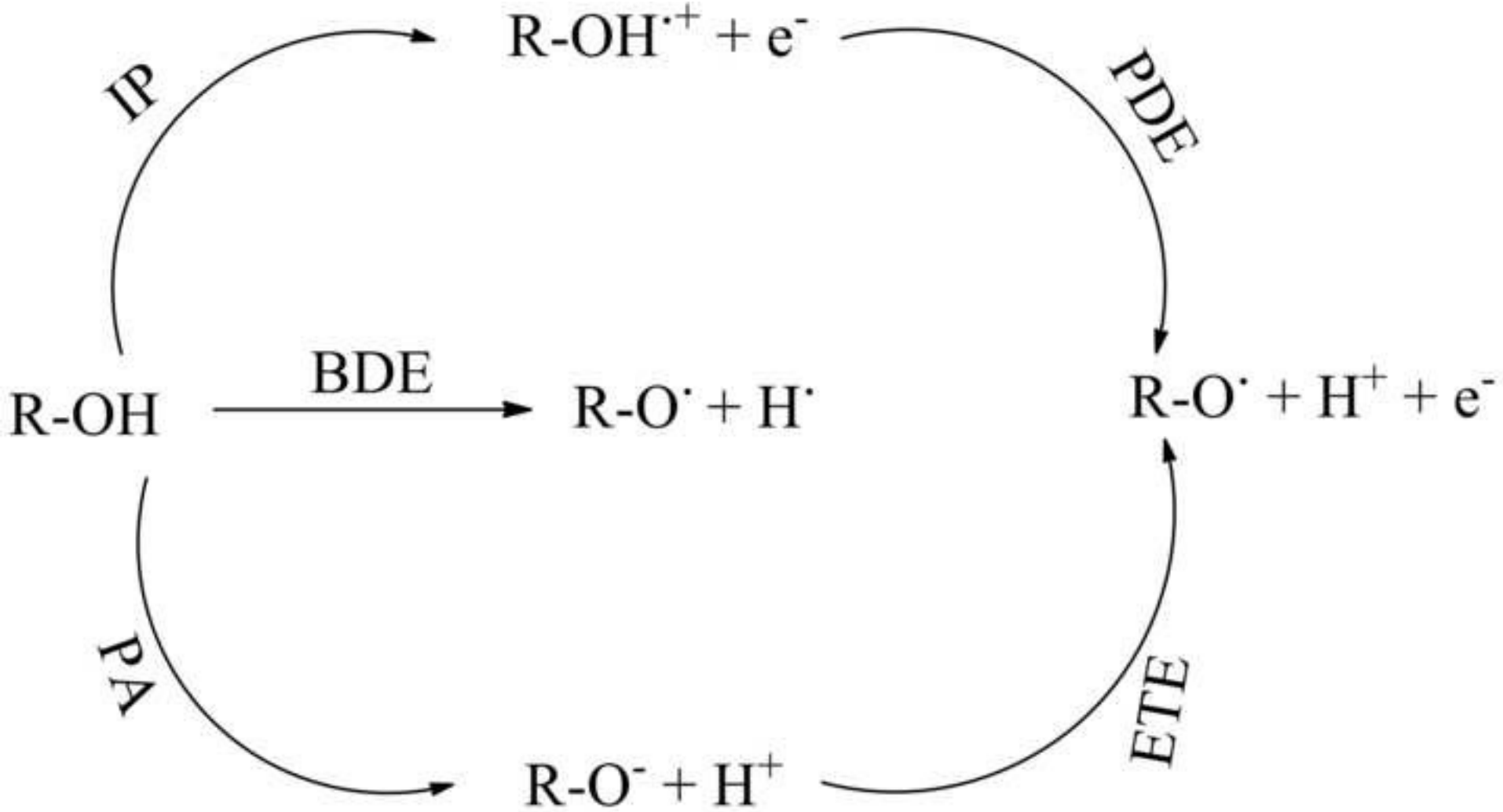

Figure 4

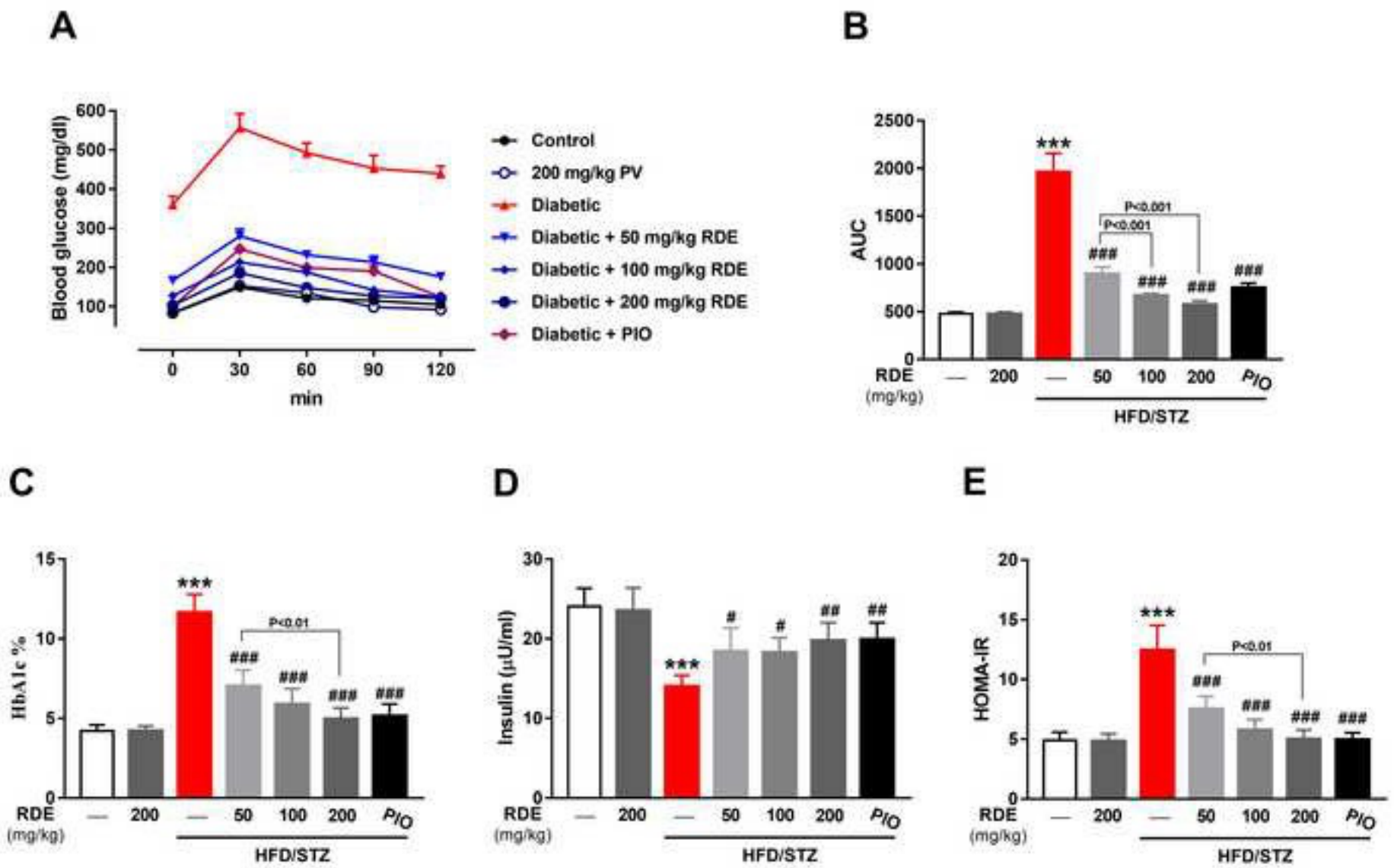
A
Blood glucose (mg/dl)
600
500
400
300
200
100
0
30
60
90
120
min
Control
200 mg/kg PV
Diabetic
Diabetic + 50 mg/kg RDE
Diabetic + 100 mg/kg RDE
Diabetic + 200 mg/kg RDE
Diabetic + PIO
B
AUC
2500
2000
1500
1000
500
0
***
P<0.001
P<0.001
###
RDE
(mg/kg)
—
200
—
50
100
200
PIO
HFD/STZ
C
HbA1c %
15
10
5
0
***
P<0.01
###
D
Insulin (μU/ml)
30
20
10
0
***
#
##
E
HOMA-IR
20
15
10
5
0

Figure 5

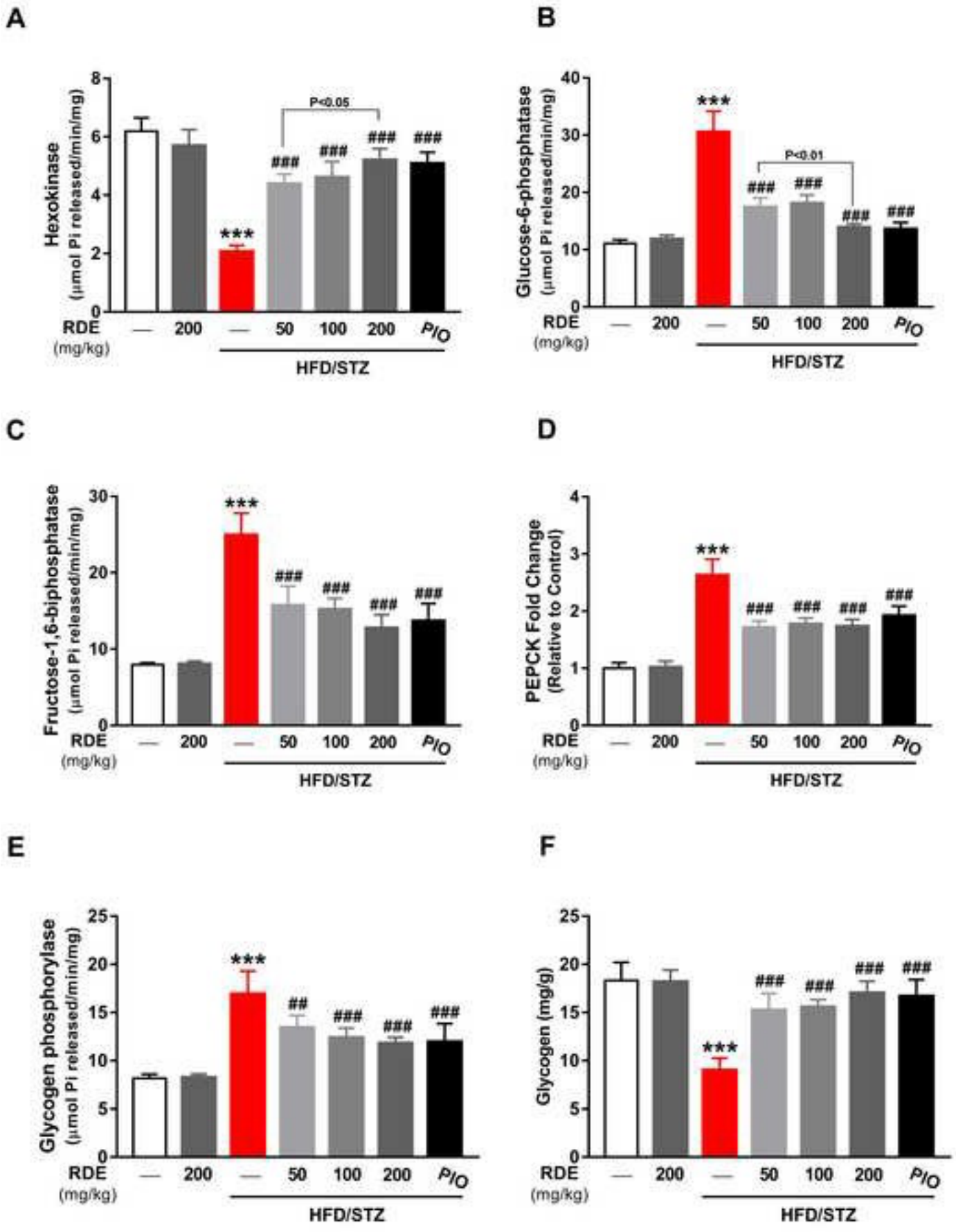
A
Hexokinase
(µmol Pi released/min/mg)
P<0.05
***
###
RDE
(mg/kg)
—
200
—
50
100
200
PIO
HFD/STZ
B
Glucose-6-phosphatase
(µmol Pi released/min/mg)
P<0.01
C
Fructose-1,6-biphosphatase
(µmol Pi released/min/mg)
D
PEPCK Fold Change
(Relative to Control)
E
Glycogen phosphorylase
(µmol Pi released/min/mg)
##
F
Glycogen (mg/g)

Figure 6

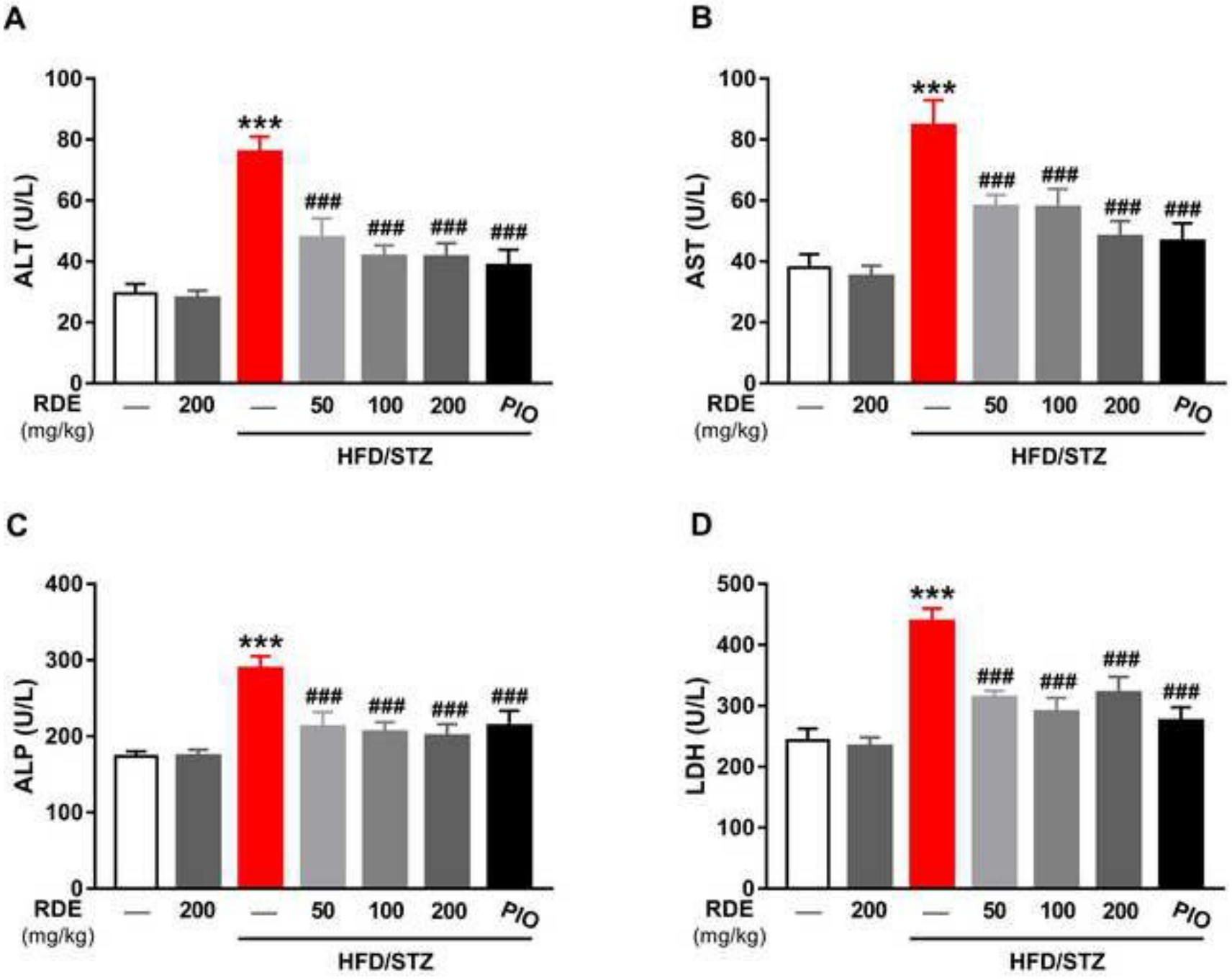
A
ALT (U/L)
100
80
60
40
20
0
***
###
###
###
###
RDE
(mg/kg)
—
200
—
50
100
200
PIO
HFD/STZ
B
AST (U/L)
100
80
60
40
20
0
***
###
###
###
###
RDE
(mg/kg)
—
200
—
50
100
200
PIO
HFD/STZ
C
ALP (U/L)
400
300
200
100
0
***
###
###
###
###
RDE
(mg/kg)
—
200
—
50
100
200
PIO
HFD/STZ
D
LDH (U/L)
500
400
300
200
100
0
***
###
###
###
###
RDE
(mg/kg)
—
200
—
50
100
200
PIO
HFD/STZ

Figure 7

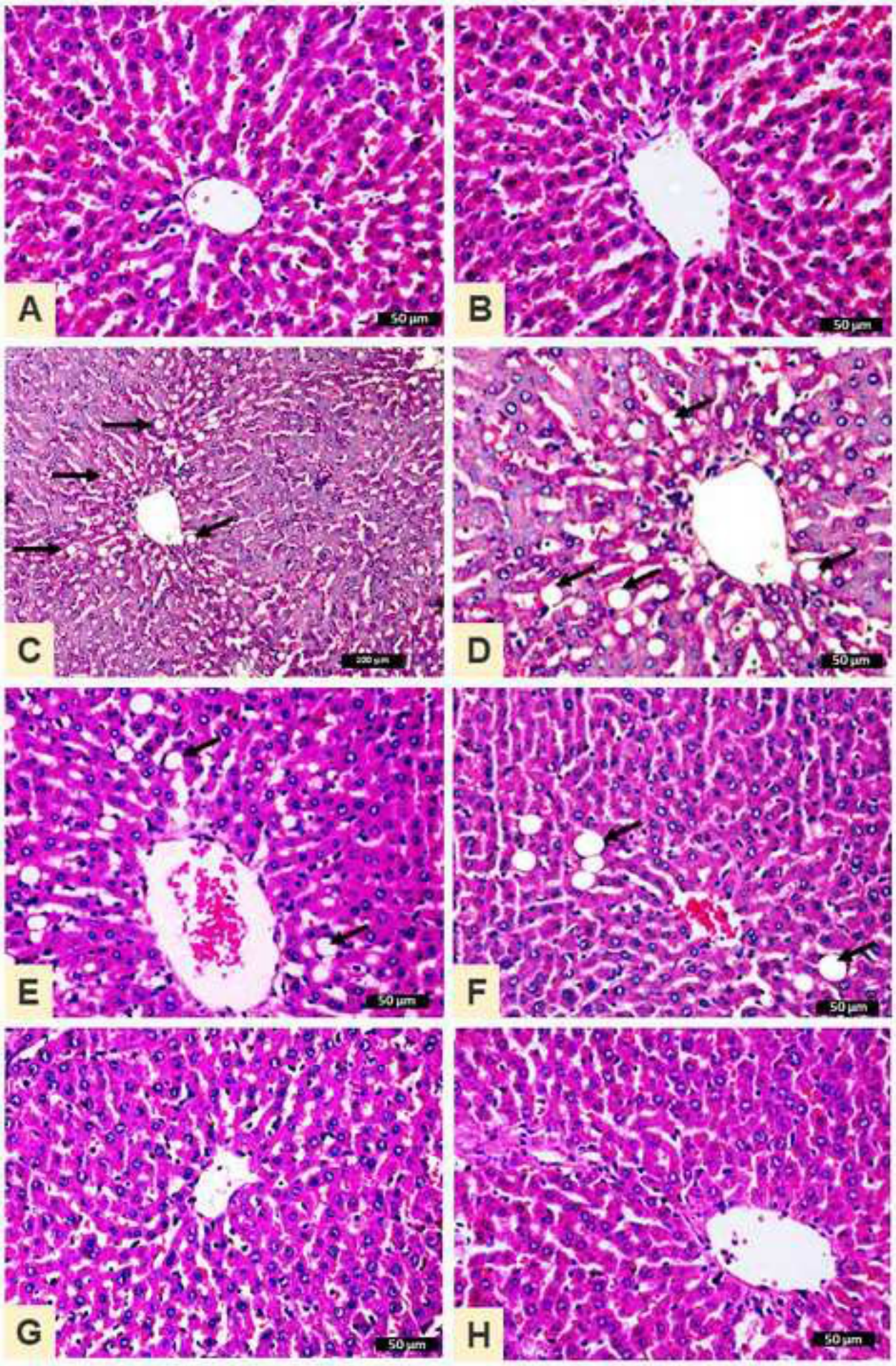

Figure 8

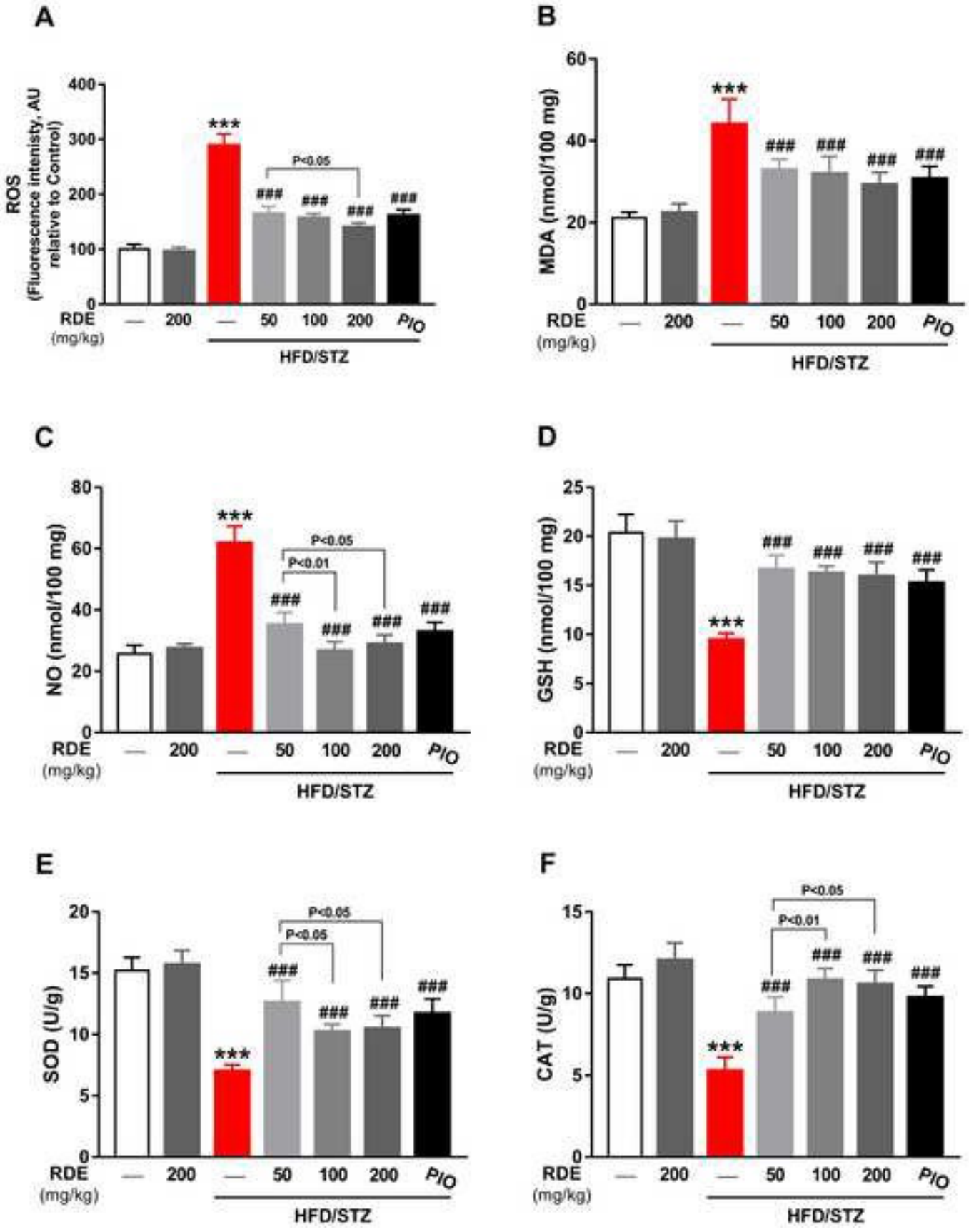
A
ROS
(Fluorescence intenisty, AU relative to Control)
400
300
200
100
0
***
P<0.05
###
RDE
(mg/kg)
—
200
—
50
100
200
PIO
HFD/STZ
B
MDA (nmol/100 mg)
60
40
20
0
C
NO (nmol/100 mg)
80
60
40
20
0
P<0.01
D
GSH (nmol/100 mg)
25
20
15
10
5
0
E
SOD (U/g)
F
CAT (U/g)

Figure 9

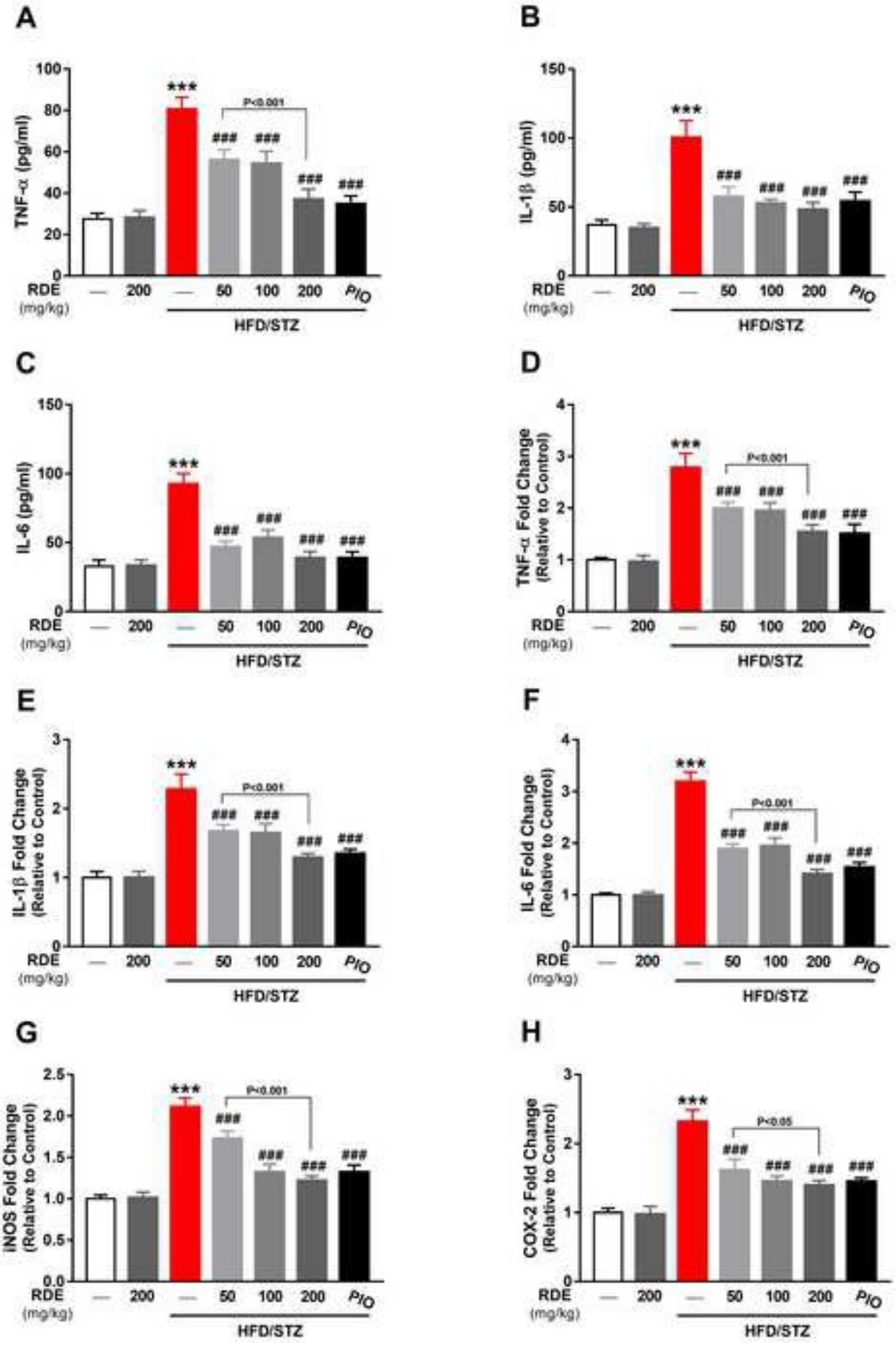
A
TNF-α (pg/ml)
B
IL-1β (pg/ml)
C
IL-6 (pg/ml)
D
TNF-α Fold Change (Relative to Control)
E
IL-1β Fold Change (Relative to Control)
F
IL-6 Fold Change (Relative to Control)
G
iNOS Fold Change (Relative to Control)
H
COX-2 Fold Change (Relative to Control)
RDE (mg/kg)
—
200
—
50
100
200
PIO
HFD/STZ
***
###
P<0.001
P<0.05

Figure 10

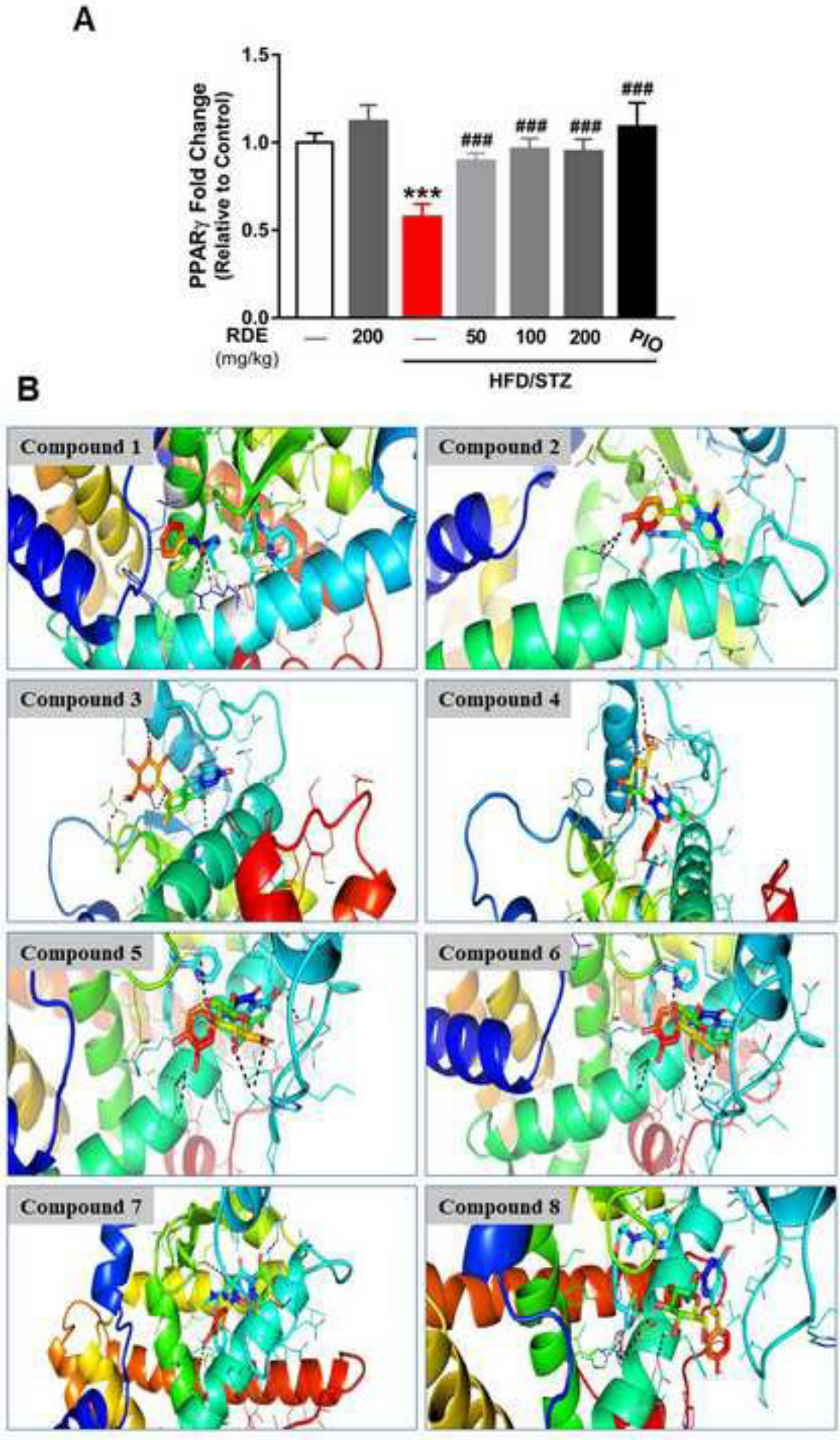
A
PPARγ Fold Change (Relative to Control)
1.5
1.0
0.5
0.0
***
###
###
###
###
RDE (mg/kg)
—
200
—
50
100
200
PIO
HFD/STZ
B
Compound 1
Compound 2
Compound 3
Compound 4
Compound 5
Compound 6
Compound 7
Compound 8